Electronic Supplementary Information

Enhanced single-molecule magnetism in dysprosium complexes of a pristine cyclobutadienyl ligand

James P. Durrant,[a,b] Jinkui Tang,[c] Akseli Mansikkamäki,*[d] and Richard A. Layfield*[a]

a. Department of Chemistry, School of Life Sciences, University of Sussex, Brighton, BN1 9QR, U.K. E-mail: R.Layfield@sussex.ac.uk
b. School of Chemistry, The University of Manchester, Oxford Road, Manchester, M13 9PL, U.K.
c. Changchun Institute of Applied Chemistry, Chinese Academy of Sciences, Renmin Street 5626, 130022 Changchun, China
d. NMR Research Unit, University of Oulu, P. O. Box 8000, FI-90014, Finland. E-mail: Akseli.Mansikkamaki@oulu.fi

Contents

General considerations

All reactions were carried out under rigorous anaerobic, anhydrous conditions under argon or nitrogen atmospheres and standard Schlenk or glove-box techniques. All solvents were refluxed over an appropriate drying agent for a minimum of three days (molten potassium for benzene, THF, D_8-THF, and Na/K alloy for hexane), and then distilled, degassed via a minimum of three freeze-pump-thaw cycles, and stored in ampoules over potassium mirrors (benzene and hexane) or activated 4 Å molecular sieves (THF, D_8-THF). Elemental analyses were carried out at MEDAC Ltd. (Surrey, U.K.) and London Metropolitan University (London, U.K.). NMR spectra were recorded on a Varian VNMR S400 spectrometer operating at 30°C unless otherwise stated at frequencies of 400 MHz (^{1}H), 128 MHz (^{11}B), 100 MHz (^{13}C), 106 MHz (^{23}Na) and 80 MHz (^{29}Si). Literature procedures were used to synthesize $[Ln(BH_4)_3(THF)_3]$ (Ln = Y, Dy), $C_4(SiMe_3)_4$, $[K_2\{C_4(SiMe_3)_4\}]$, and $[Na_2\{C_4(SiMe_3)_4\}THF]_2$.[1-4]

Synthesis of $[Y\{\eta^4\text{-}C_4(SiMe_3)_4\}(BH_4)_2(THF)Na]$ ($\mathbf{1_Y}$). A solution of $[Na_2\{C_4(SiMe_3)_4\}THF]_2$ (200 mg, 0.44 mmol) in benzene (20 mL) was added dropwise to a solution of $[Y(BH_4)_3(THF)_3]$ (152 mg, 0.44 mmol) in benzene (20 mL). The resulting dark red solution was swirled and left to stand for 20 hours, by which time yellow crystals of $\mathbf{1_Y}$ suitable for X-ray crystallography were obtained from the crude reaction mixture (155 mg, 64 %). ^{1}H NMR (δ/ppm): 3.62 (m, CH_2O, 4H), 1.77 (m, CH_2, 4H), 0.50 (bs, BH_4, 2H), 0.30 (bs, BH_4, 2H), 0.13 (s, $SiMe_3$, 36H), −0.12 (bs, BH_4, 2H). The two protons corresponding to the other BH environments occur under the $SiMe_3$ peak and satellites and so could not be integrated. ^{13}C{^{1}H} NMR (δ/ppm): 122.63 (C_4 ring), 68.38 (CH_2O), 26.49 (CH_2), 5.28 ($SiMe_3$). ^{11}B{^{1}H} NMR (δ/ppm): −23.00 (bs, BH_4). ^{11}B NMR (δ/ppm): −23.00 (bs, BH_4).^{29}Si{^{1}H} NMR (δ/ppm): −22.69. ^{23}Na NMR (δ/ppm): −4.26. FTIR ($\bar{\nu}$/cm^{-1}): 3000-2850 (m, b, C-H), 2450 (m, s, B-H_T), 2300-2100 (m, b, B-H_B). Despite repeated attempts, satisfactory elemental analysis could not be obtained for this compound, a representative result being (%), found (calculated) for $C_{20}H_{52}YNaB_2Si_4O$: C 35.90 (43.32); H 8.76 (9.45). However, the NMR spectroscopic analysis (Figures S1-S6 and S12) of this compound is consistent with the molecular structure determined by X-ray crystallography.

Synthesis of $[Dy\{\eta^4\text{-}C_4(SiMe_3)_4\}(BH_4)_2(THF)Na]$ ($\mathbf{1_{Dy}}$). Compound $\mathbf{1_{Dy}}$ was synthesised by following the same procedure as for $\mathbf{1_Y}$ using $[Na_2\{C_4(SiMe_3)_4\}THF]_2$ (237 mg, 0.52 mmol) and $[Dy(BH_4)_3(THF)_3]$ (219 mg, 0.52

mmol). Yellow crystals of $\mathbf{1_{Dy}}$ suitable for X-ray crystallography were obtained from the crude reaction mixture (156 mg, 48 %). FTIR ($\bar{\nu}$/cm^{-1}): 3000-2850 (m, b, C-H), 2450 (m, s, B-H$_T$), 2300-2100 (m, b, B-H$_B$). Elemental analysis (%), found (calculated) for $C_{20}H_{52}DyNaB_2Si_4O$: C 37.66 (38.25); H 8.50 (8.35).

Synthesis of [Y{η^4-C$_4$(SiMe$_3$)$_4$}(BH$_4$)$_2$(THF)K] ($\mathbf{2_Y}$). A solution of [K$_2${C$_4$(SiMe$_3$)$_4$}] (200 mg, 0.48 mmol) in benzene (20 mL) was added dropwise to a solution of [Y(BH$_4$)$_3$(THF)$_3$] (167 mg, 0.48 mmol) in benzene (20 mL). The resulting dark red solution was swirled and left to stand for 20 hours, by which time a yellow precipitate (with some crystalline material) had deposited. The benzene was decanted and the resulting solid was washed with hexane (3 × 20 mL), extracted with THF (2 × 20 mL) and filtered. The solvent was removed in *vacuo* to give a yellow powder subsequently identified as $\mathbf{2_Y}$ (194 mg, 71 %). Pale yellow crystals of $\mathbf{2_Y}$ suitable for single-crystal X-ray diffraction were obtained by the slow evaporation of layered hexane on a saturated THF solution over five days (151 mg, 56 %). ^{1}H NMR (δ/ppm): 3.62 (m, CH$_2$O, 4H), 1.77 (m, CH$_2$, 4H), 0.60 (bs, BH$_4$, 2H), 0.39 (bs, BH$_4$, 2H), 0.18 (bs, BH$_4$, 2H), 0.14 (s, SiMe$_3$, 36H), −0.02 (bs, BH$_4$, 2H). ^{13}C{^{1}H} NMR (δ/ppm): 123.32 (d, $^1J_{CY}$ = 4.45 Hz, C$_4$ ring), 68.37 (CH$_2$O), 26.50 (CH$_2$), 5.24 (SiMe$_3$). ^{11}B{^{1}H} NMR (δ/ppm): −27.01 (s, BH$_4$). ^{11}B NMR (δ/ppm): −27.00 (quintet, $^1J_{BH}$ = 84 Hz, BH$_4$).^{29}Si{^{1}H} NMR (δ/ppm): −22.58. FTIR ($\bar{\nu}$/cm^{-1}): 3000-2850 (m, b, C-H), 2450 (m, s, B-H$_T$), 2300-2100 (m, b, B-H$_B$). Elemental analysis (%), found (calculated) for $C_{20}H_{52}YKB_2Si_4O$: C 41.12 (42.10); H 8.73 (9.19).

Synthesis of [Dy{η^4-C$_4$(SiMe$_3$)$_4$}(BH$_4$)$_2$(THF)K] ($\mathbf{2_{Dy}}$). Compound $\mathbf{2_{Dy}}$ was synthesised by following the same procedure as for $\mathbf{2_Y}$ using [K$_2${C$_4$(SiMe$_3$)$_4$}] (500 mg, 1.19 mmol) and [Dy(BH$_4$)$_3$(THF)$_3$] (505 mg, 1.19 mmol). The solvent was removed in *vacuo* to give a yellow powder subsequently identified as $\mathbf{2_{Dy}}$ (655 mg, 85 %). Yellow crystals of $\mathbf{2_{Dy}}$ suitable for X-ray crystallography were obtained by the slow evaporation of layered hexane on a saturated THF solution over five days (108 mg, 72 % based on 150 mg of crude $\mathbf{2_{Dy}}$). FTIR ($\bar{\nu}$/cm^{-1}): 3000-2850 (m, b, C-H), 2450 (m, s, B-H$_T$), 2300-2100 (m, b, B-H$_B$). Elemental analysis (%), found (calculated) for $C_{20}H_{52}DyKB_2Si_4O$: C 37.13 (37.29); H 8.04 (8.14).

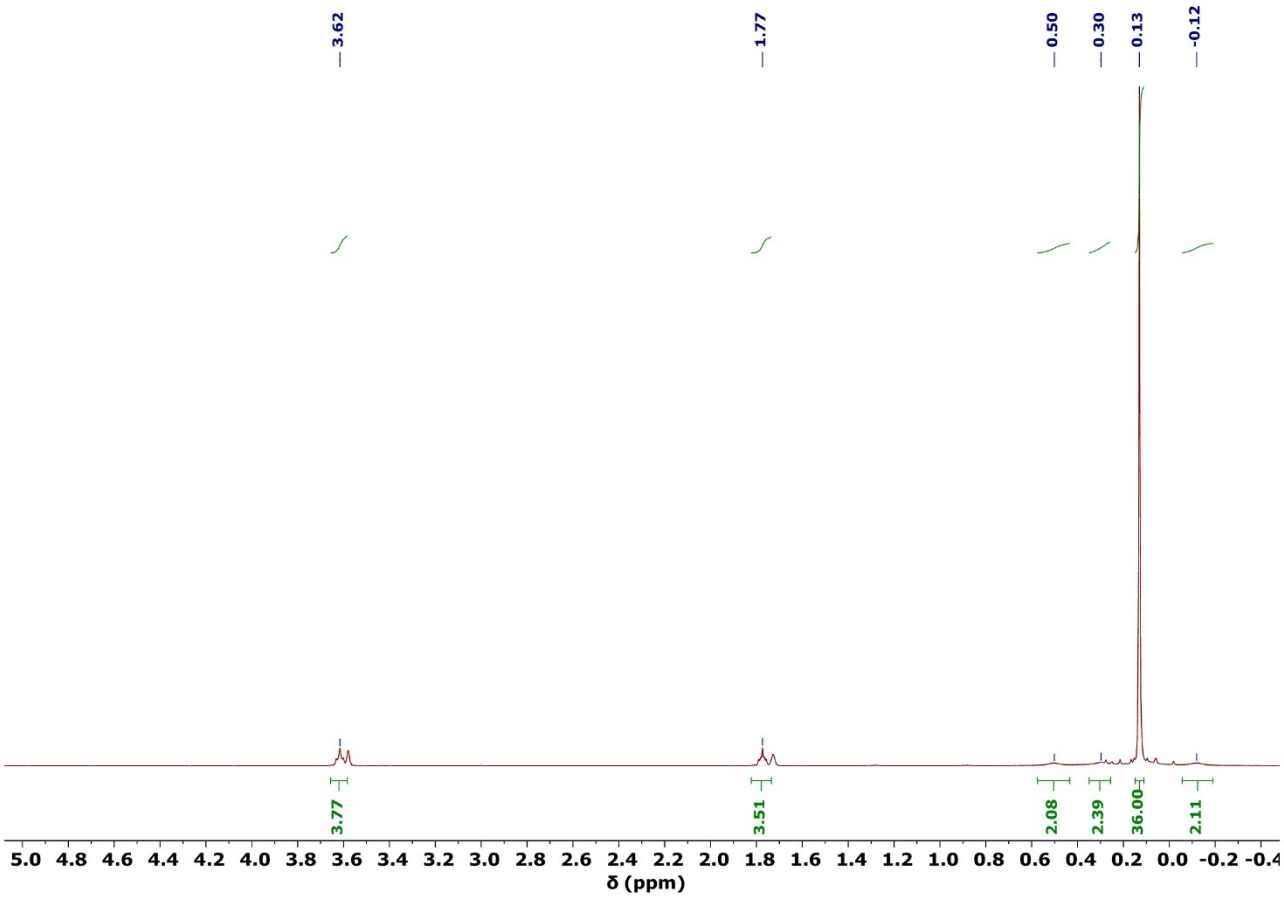

Figure S1. ^{1}H NMR spectrum of $\mathbf{1_Y}$ in D_8-THF.

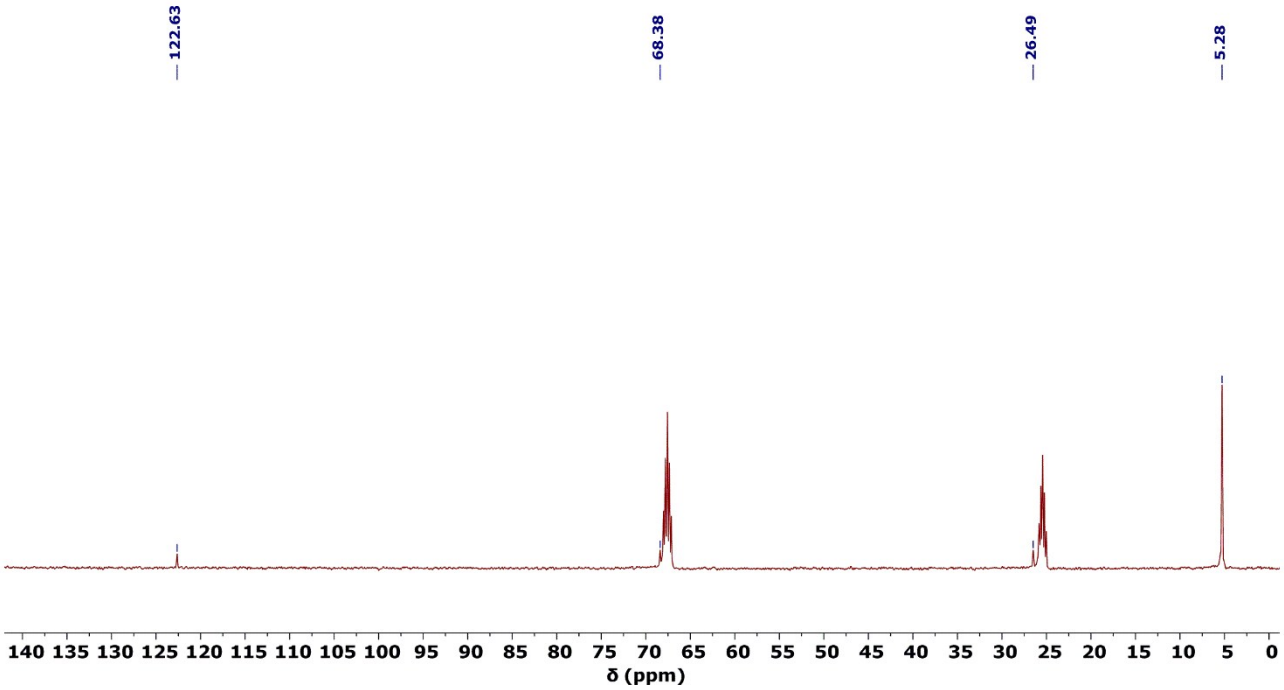

Figure S2. ^{13}C NMR spectrum of $\mathbf{1_Y}$ in D_8-THF.

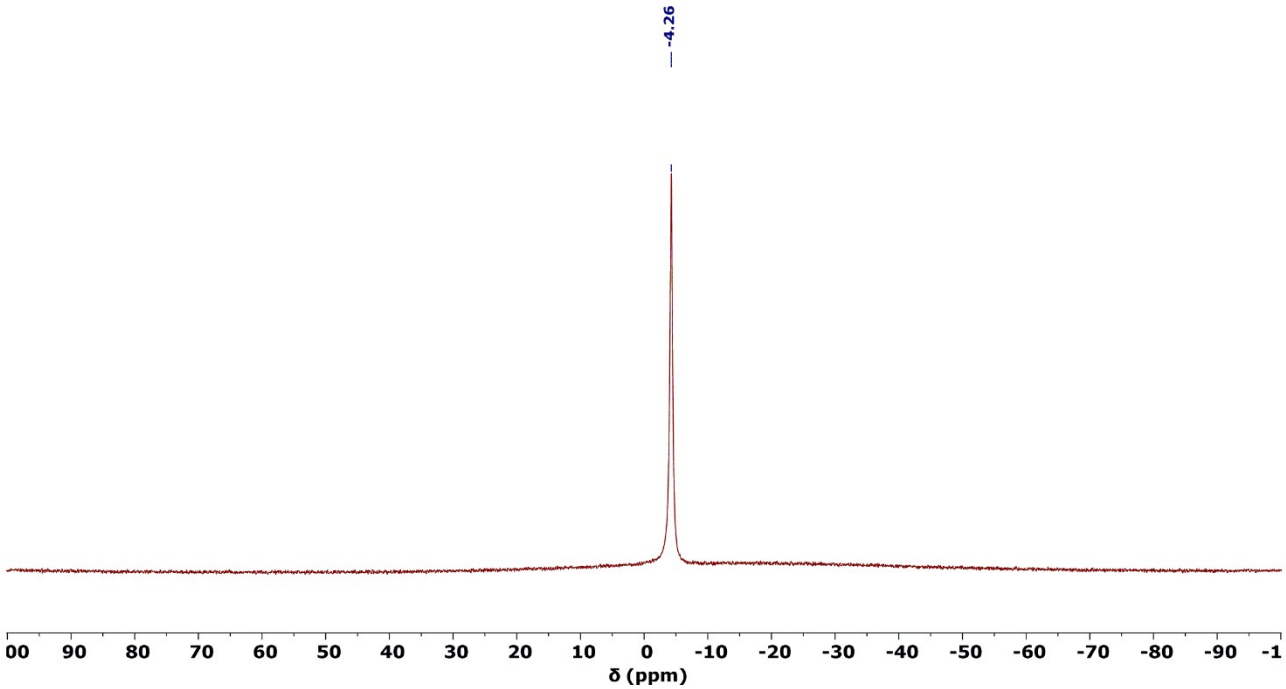

Figure S3. ^{23}Na NMR spectrum of $\mathbf{1_Y}$ in D_8-THF.

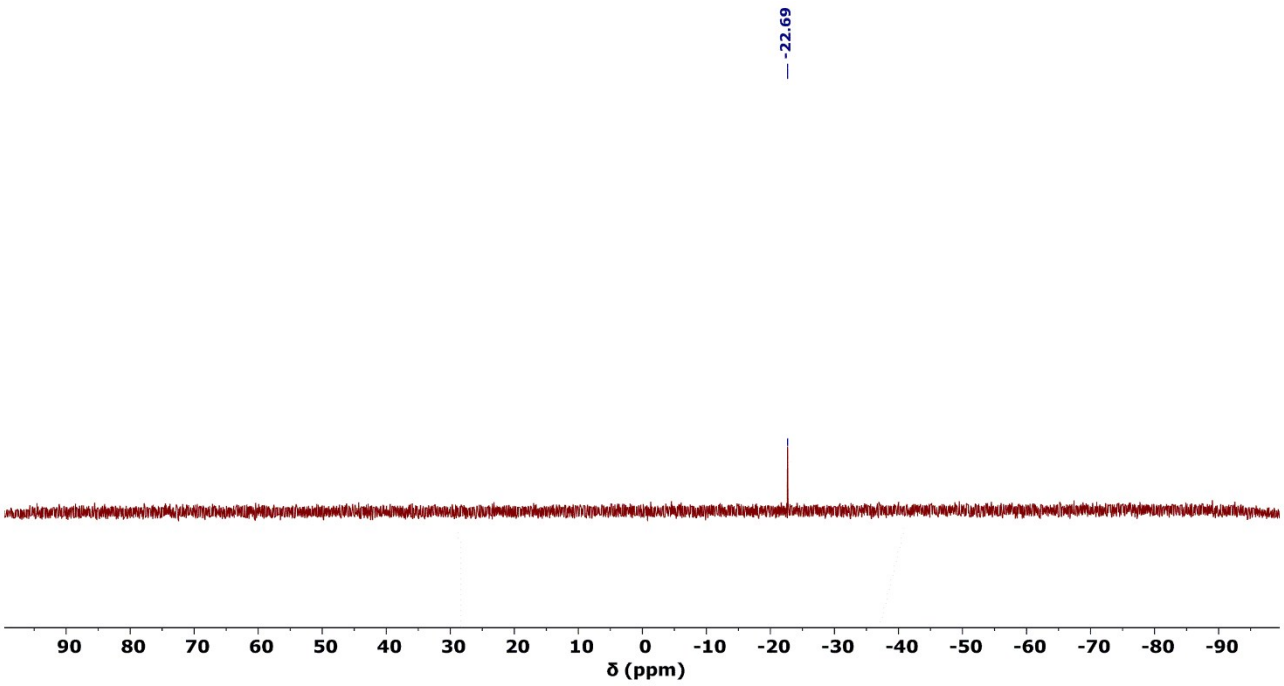

Figure S4. ^{29}Si NMR spectrum of **1$_Y$** in D_8-THF.

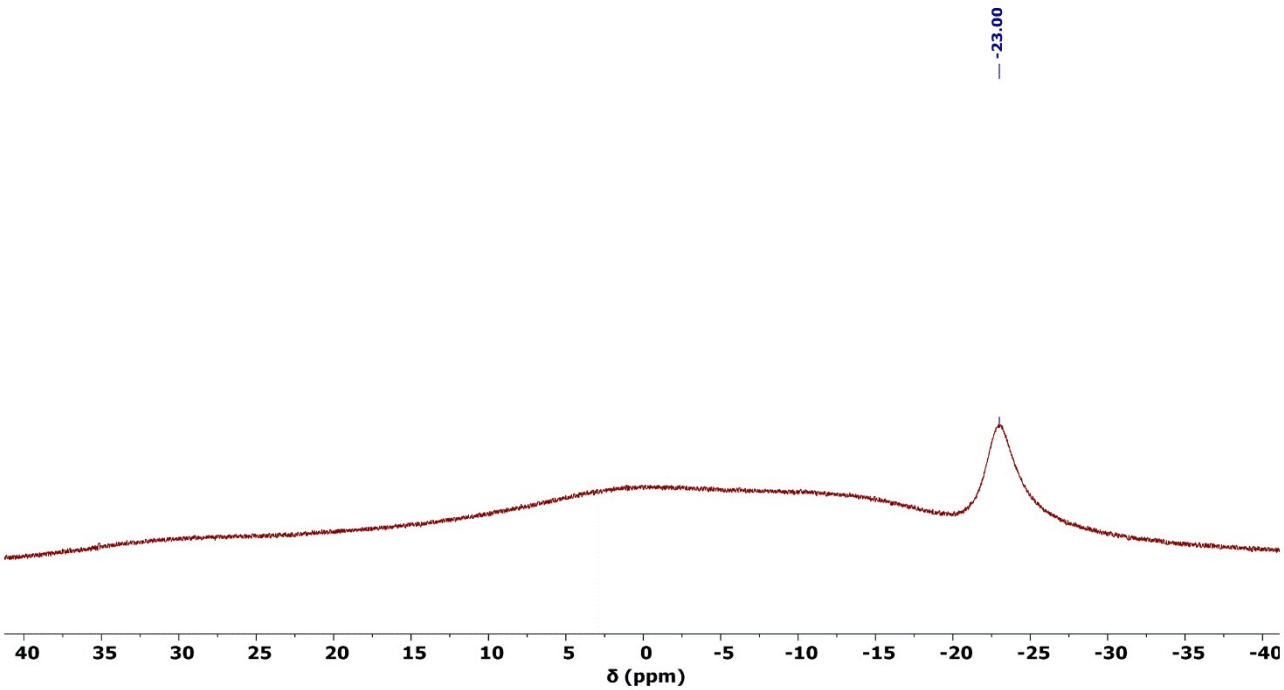

Figure S5. $^{11}B\{^{1}H\}$ NMR spectrum of $\mathbf{1_Y}$ in D_8-THF.

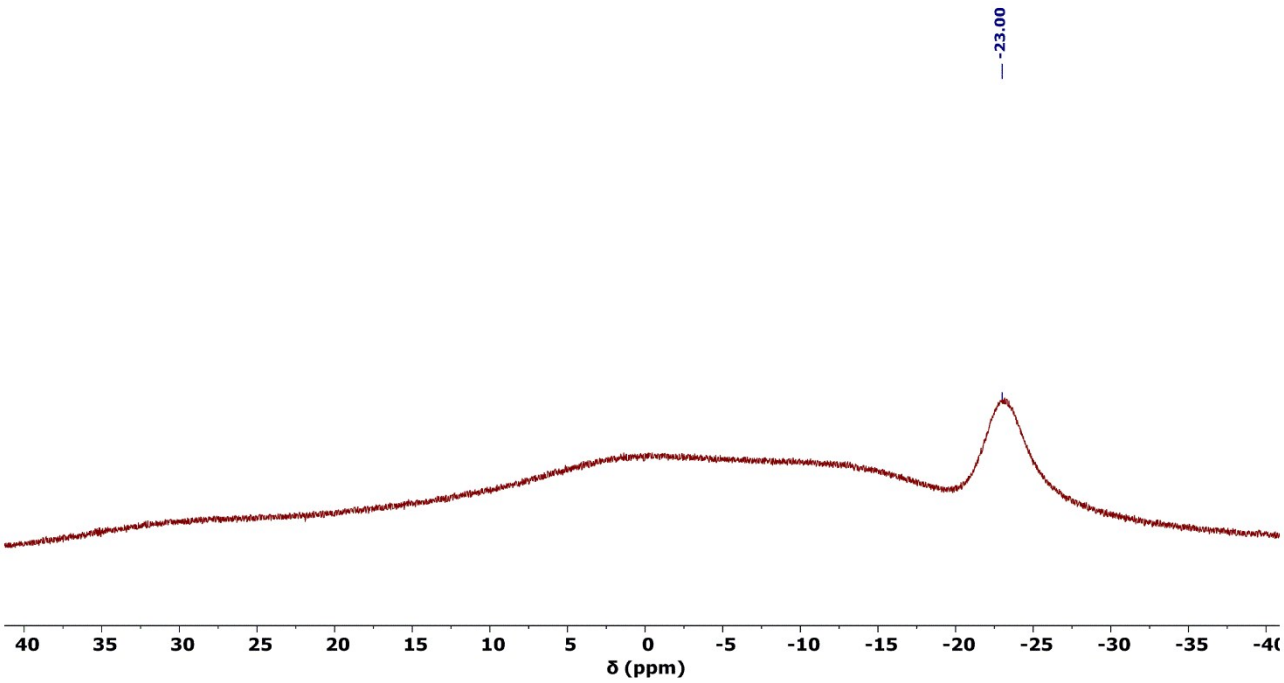

Figure S6. ^{11}B NMR spectrum of $\mathbf{1_Y}$ in D_8-THF.

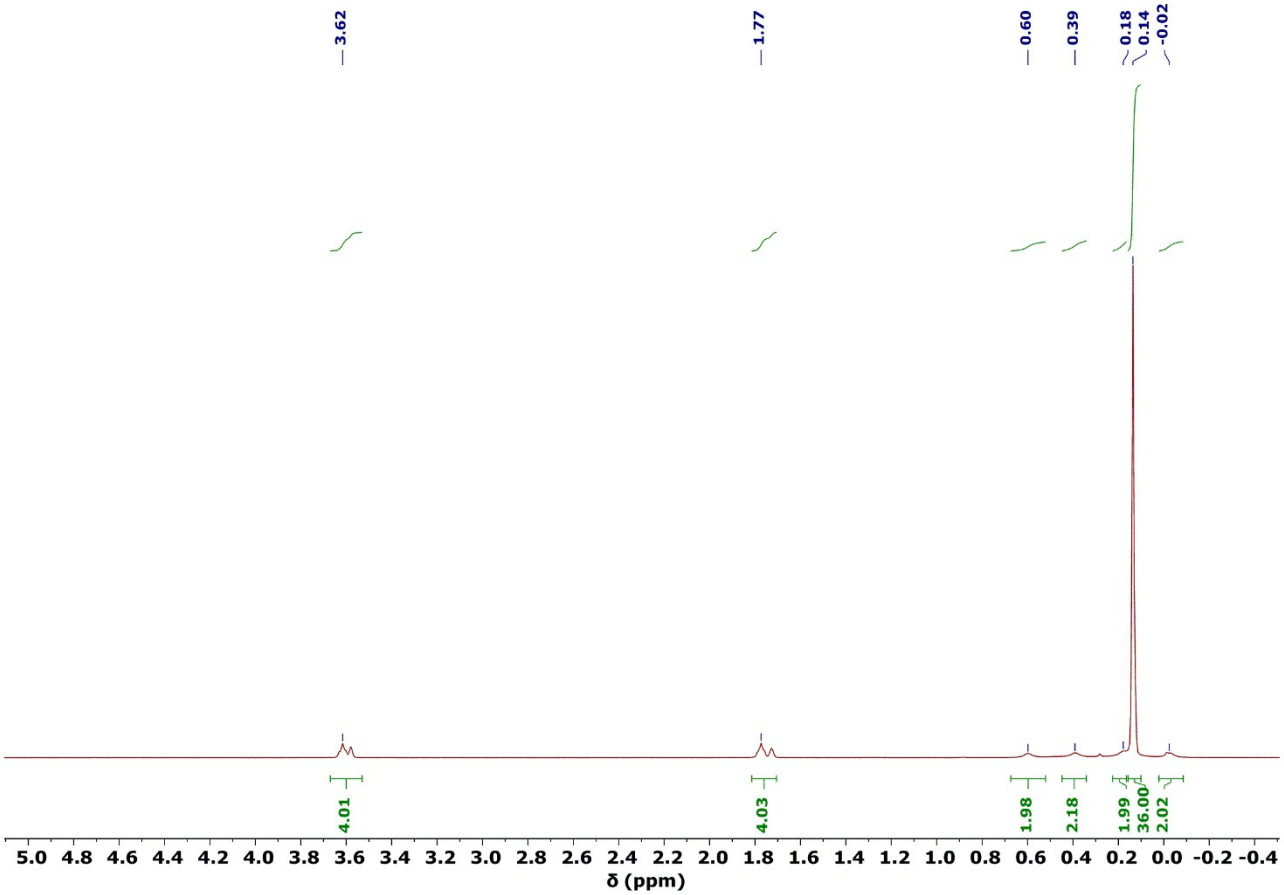

Figure S7. ^{1}H NMR spectrum of $\mathbf{2_Y}$ in D_8-THF.

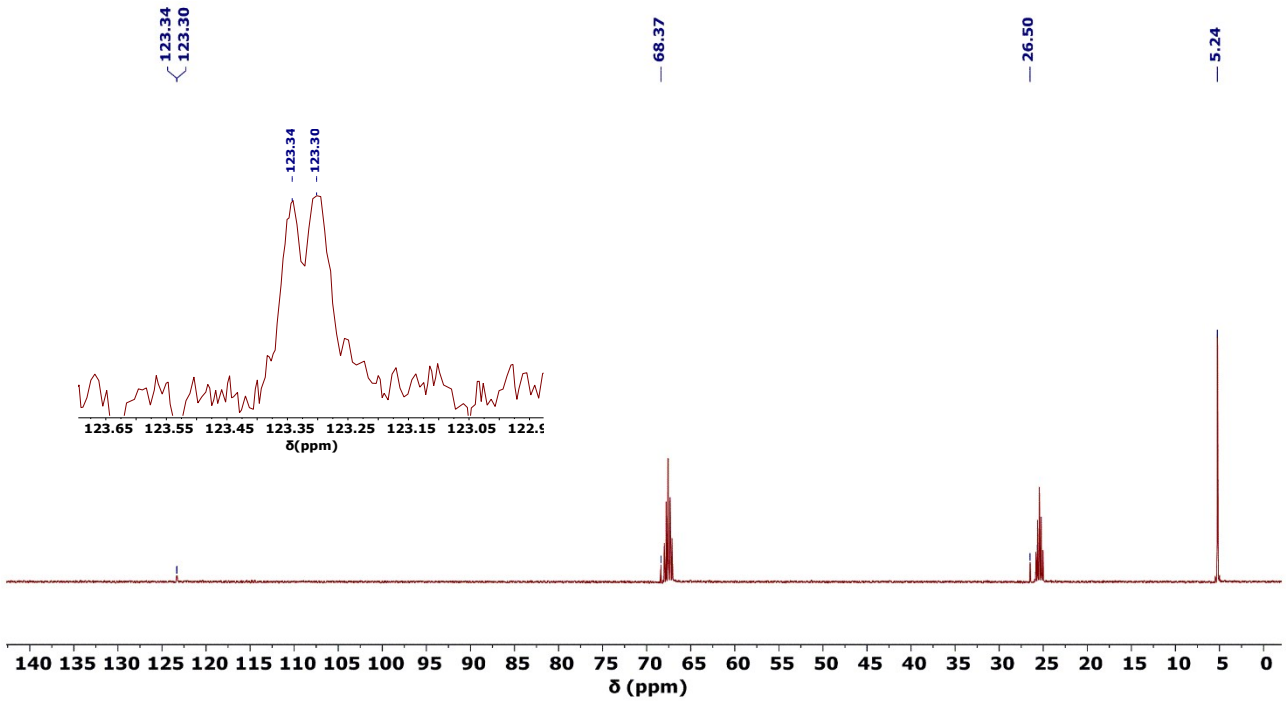

Figure S8. ^{13}C NMR spectrum of $\mathbf{2_Y}$ in D_8-THF. Inset: expansion of the peak corresponding to the C_4 ring carbon atoms coupled to ^{89}Y.

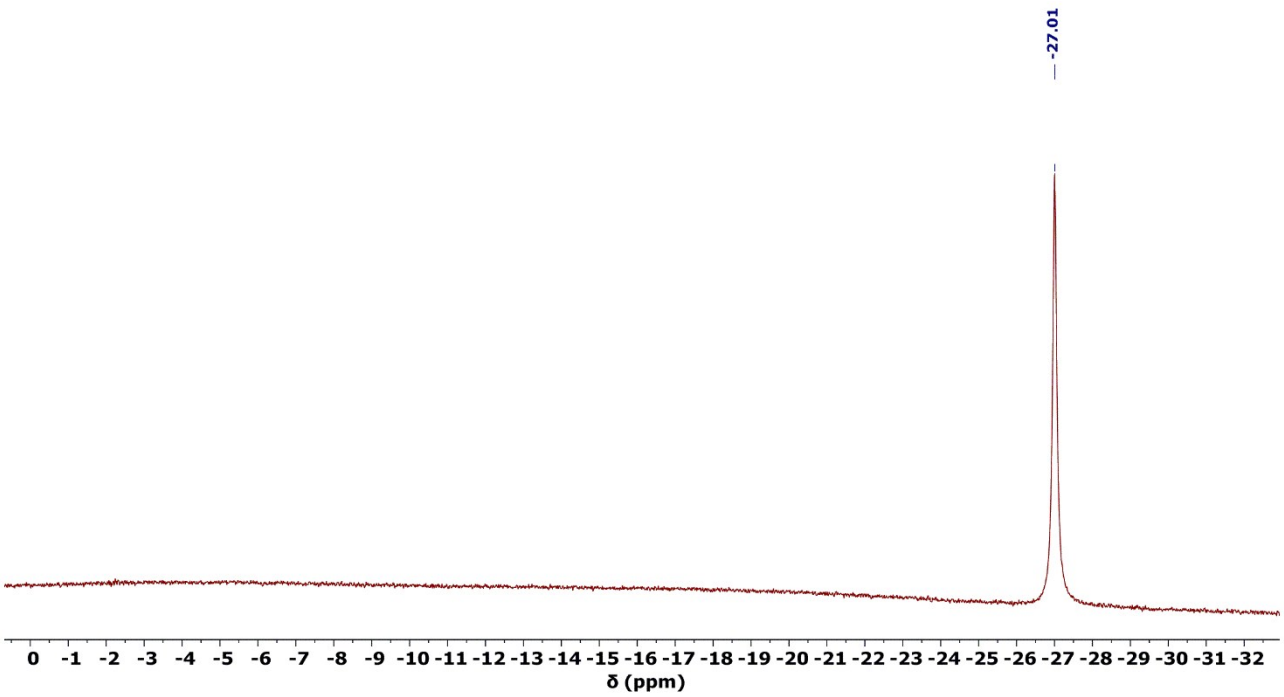

Figure S9. $^{11}B\{^{1}H\}$ NMR spectrum of $\mathbf{2_Y}$ in D_8-THF.

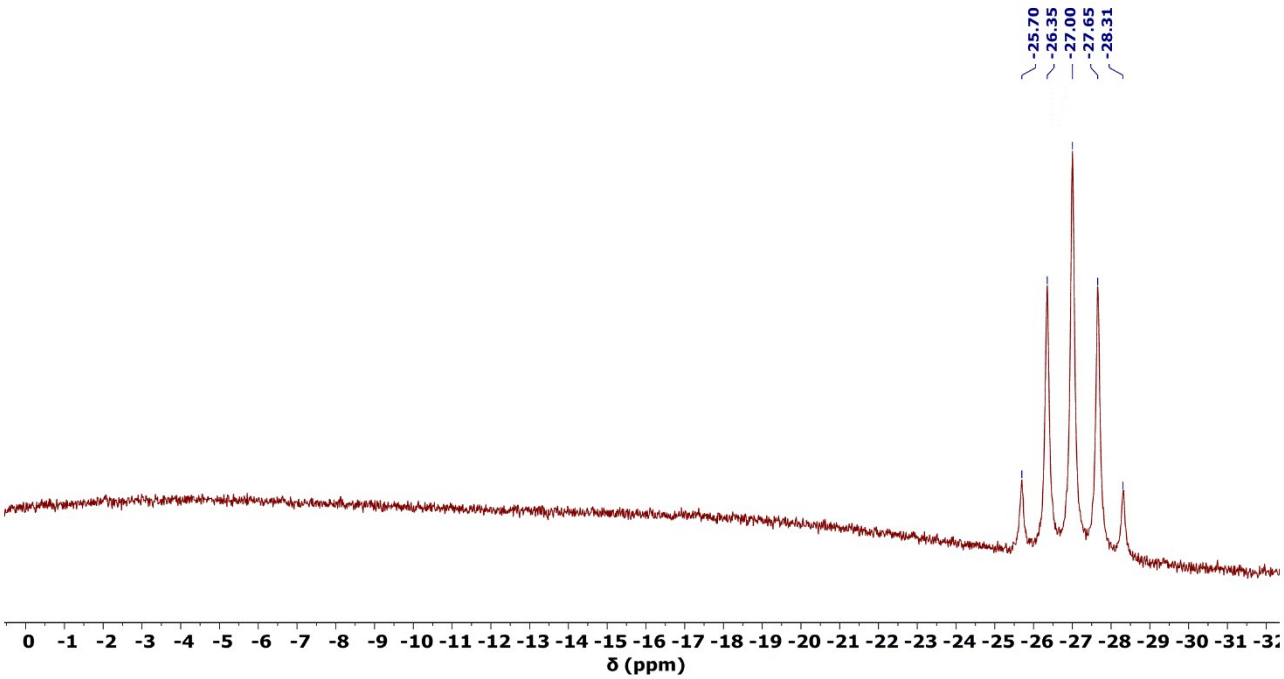

Figure S10. ^{11}B NMR spectrum of $\mathbf{2_Y}$ in D_8-THF.

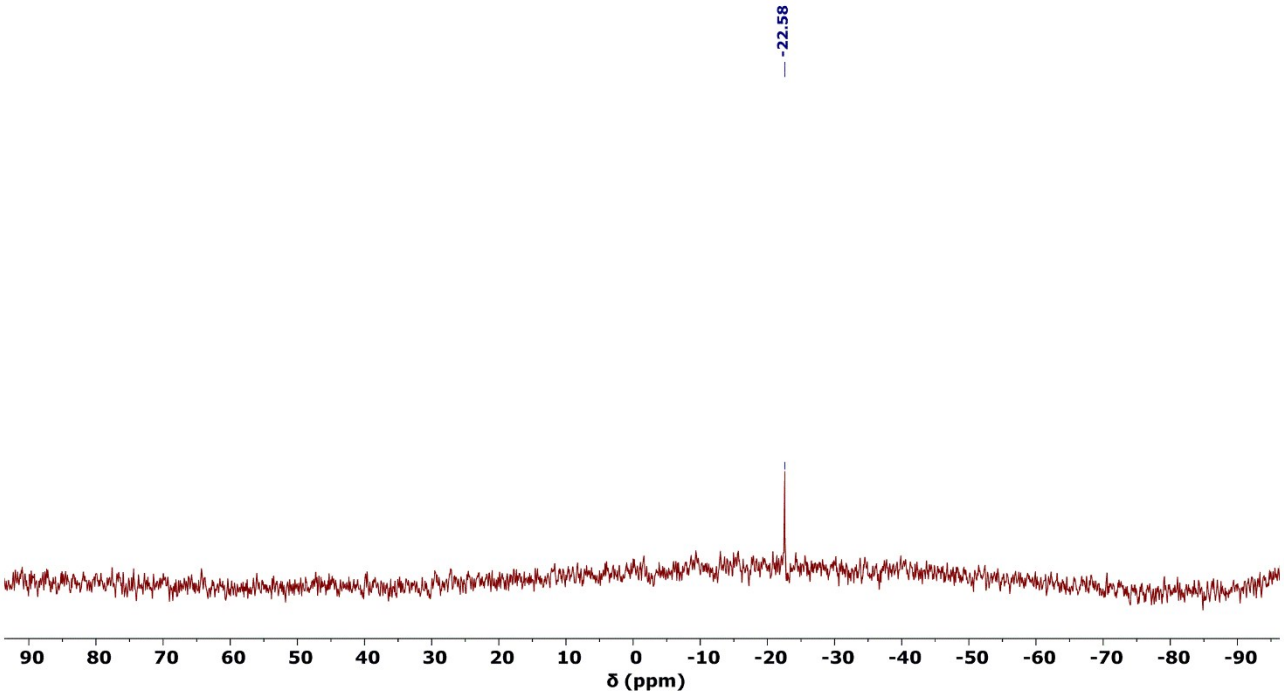

Figure S11 ^{29}Si NMR spectrum of **2$_Y$** in D_8-THF.

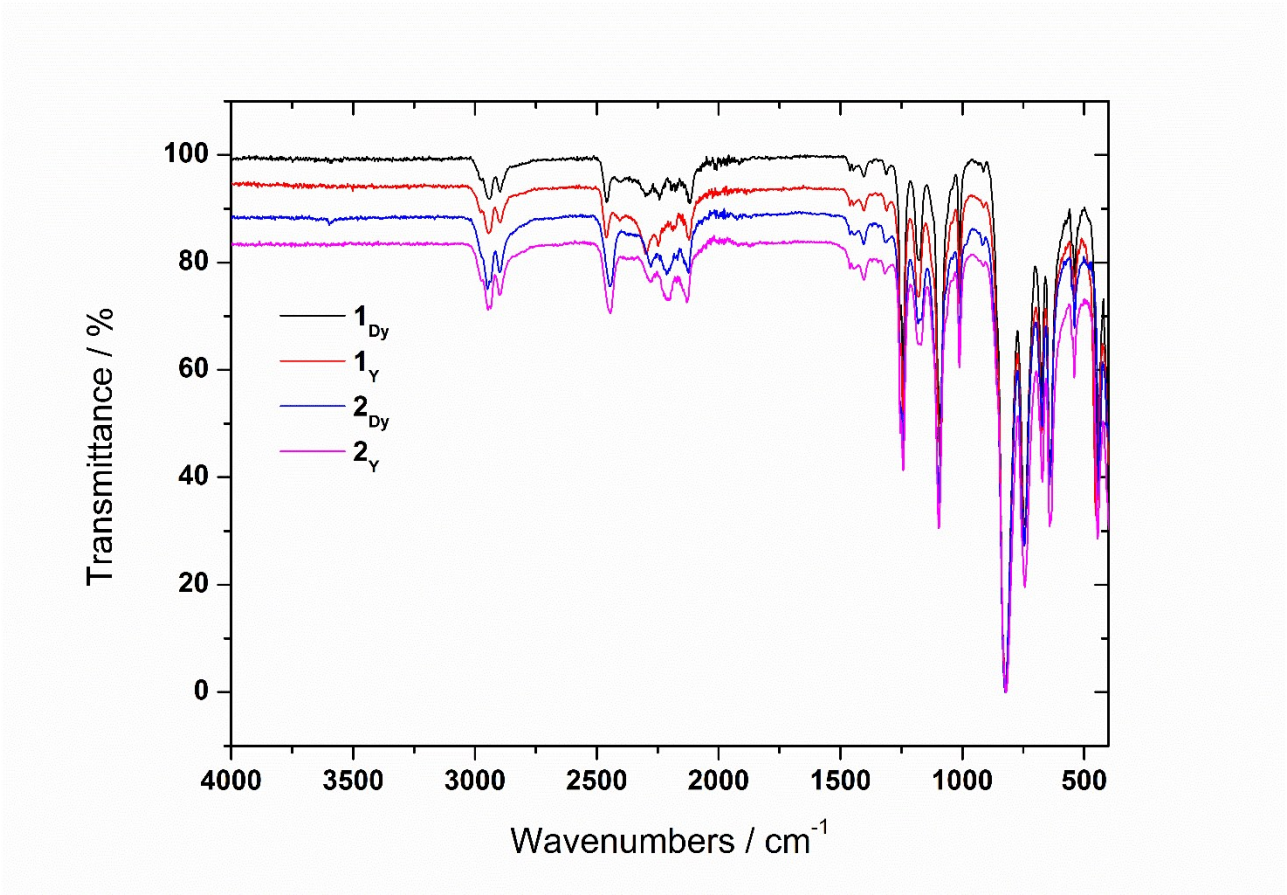

Figure S12. FTIR spectra of $\mathbf{1}_{Dy}$, $\mathbf{1}_{Y}$, $\mathbf{2}_{Dy}$ and $\mathbf{2}_{Y}$.

X-ray crystallography

Single-crystal X-ray diffraction measurements were carried out on an Agilent Gemini Ultra diffractometer using CuKα radiation (λ = 1.54184 Å) at 100 K. Structures were solved in Olex2 with SHELXT using intrinsic phasing and were refined with SHELXL using least squares minimisation.[5-7] Anisotropic thermal parameters were used for the non-hydrogen atoms and isotropic parameters for the hydrogen atoms. Hydrogen atoms on carbons were added geometrically and refined using a riding model. Crystals of $\mathbf{1_Y}$, $\mathbf{1_{Dy}}$, $\mathbf{2_Y}$ and $\mathbf{2_{Dy}}$ were all twinned, so were processed using the twinning software within CrysAlisPro. Two components were found for $\mathbf{1_{Dy}}$, $\mathbf{2_Y}$, and $\mathbf{2_{Dy}}$ (60/35 % for $\mathbf{1_{Dy}}$, 68/32 % for $\mathbf{2_Y}$ and 70/30 % for $\mathbf{2_{Dy}}$) and three components were found for $\mathbf{1_Y}$ (50/25/20 %). Data was solved using hklf 4 and refined against hklf 5. The hydrogen atoms from borohydrides were located based on residual electron density and were refined freely. In the case of $\mathbf{2_{Dy}}$, the B–H distances of the bridging hydrogen atoms were fixed at the same length using the SADI command.

Table S1. Crystal data and structure refinement parameters for $\mathbf{1_Y}$, $\mathbf{1_{Dy}}$, $\mathbf{2_Y}$ and $\mathbf{2_{Dy}}$.

	$\mathbf{1_Y}$	$\mathbf{1_{Dy}}$	$\mathbf{2_Y}$	$\mathbf{2_{Dy}}$
CCDC ref. code	1987236	1987237	1987238	1987239
empirical formula	$C_{40}H_{104}Y_2Na_2B_4Si_8O_2$	$C_{40}H_{104}Dy_2Na_2B_4Si_8O_2$	$C_{20}H_{52}YKB_2Si_4O$	$C_{20}H_{52}DyKB_2Si_4O$
formula weight	1108.99	1256.17	570.60	644.19
crystal system	triclinic	triclinic	monoclinic	monoclinic
space group	*P*–1	*P*–1	$P2_1/n$	$P2_1/n$
a (Å)	10.929(2)	10.9592(4)	10.7817(4)	10.8460(3)
b (Å)	16.497(4)	16.5329(8)	17.5986(5)	17.5547(4)
c (Å)	17.2819(10)	17.2892(7)	16.9013(6)	16.9092(3)
α (°)	90.747(10)	90.676(4)	90	90
β (°)	90.198(11)	90.257(3)	91.955(3)	91.916(2)
γ (°)	92.00(2)	92.791(4)	90	90
V (Å^3)	3113.7(11)	3128.6(2)	3205.03(19)	3217.68(13)
Z	2	2	4	4
T (K)	100	100	100	100
ρ_{calc} (g/cm^3)	1.183	1.333	1.183	1.330
F (000)	1184.0	1292.0	1216.0	1324.0
Reflections collected	24473	17751	11390	10395
Independent reflections	24473	17751	11390	10395
R_{int} [†]	17.63	15.52	6.27	6.85
GOF on F^2	1.047	0.933	0.855	0.902
R_1 [a]	0.0736	0.0604	0.0341	0.0458
R_w [b]	0.2307	0.1524	0.0765	0.1140

[a] $R_1[I>2\sigma(I)] = \sum||F_o|-|F_c||/\sum|F_o|$; [b] $R_w[\text{all data}] = [\sum\{w(F_o^2-F_c^2)^2\}/\sum\{w(F_o^2)^2\}]^{1/2}$

[†] Based on hklf 4.

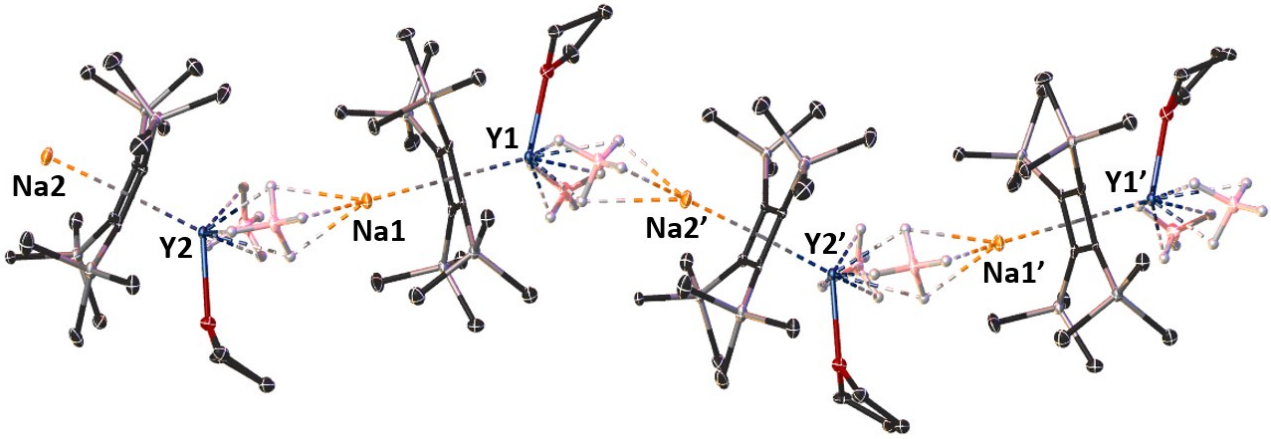

Figure S13. Thermal ellipsoid representations (50% probability) of a segment of the polymeric structure of $\mathbf{1}_{\mathbf{Y}}$. H = white, B = pink, C = black, O = red, Na = orange, Si = grey, Dy = green. For clarity, only the hydrogen atoms bound to boron are shown.

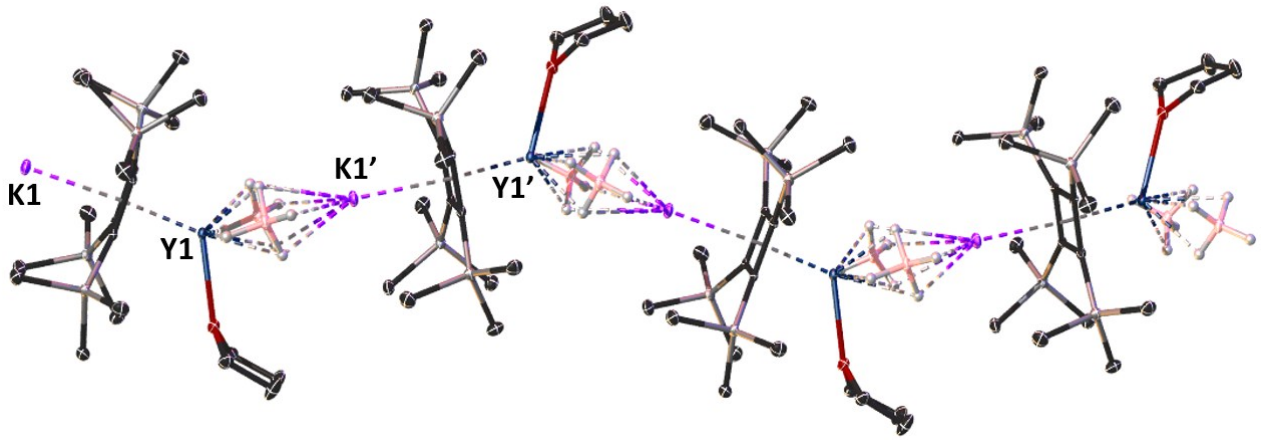

Figure S14. Thermal ellipsoid representations (50% probability) of a segment of the polymeric structure of $\mathbf{2}_{\mathbf{Y}}$. H = white, B = pink, C = black, O = red, Si = grey, K = lilac, Dy = green. For clarity, only the hydrogen atoms bound to boron are shown.

Table S2. Selected bond lengths and angles for $\mathbf{1_Y}$ and $\mathbf{1_{Dy}}$.

	$\mathbf{1_Y}$	$\mathbf{1_{Dy}}$
Ln–C(η^4-Cb)/Å	Y1–C1: 2.498(10) Y1–C2: 2.485(9) Y1–C3: 2.494(9) Y1–C4: 2.500(9) Y2–C21: 2.484(10) Y2–C22: 2.517(10) Y2–C23: 2.488(10) Y2–C24: 2.481(9)	Dy1–C1: 2.489(8) Dy1–C2: 2.500(8) Dy1–C3: 2.489(9) Dy1–C4: 2.500(9) Dy2–C21: 2.485(8) Dy2–C22: 2.484(8) Dy2–C23: 2.506(9) Dy2–C24: 2.529(9)
Ln–(η^4-Cb_{cent})/Å	Y1: 2.261(5) Y2: 2.257(5)	Dy1: 2.262(4) Dy2: 2.267(4)
Na–C(η^4-Cb_{cent})/Å	Na1: 2.386(6) Na2: 2.376(6)	Na1: 2.392(6) Na2: 2.373(6)
Ln–(η^4-Cb_{cent})–Na/°	Y1–Na1: 178.1(2) Y2–Na2: 177.8(3)	Dy1–Na1: 178.4(2) Dy2–Na2: 177.7(2)

Table S3. Selected bond lengths and angles for $\mathbf{2_Y}$ and $\mathbf{2_{Dy}}$.

	$\mathbf{2_Y}$	$\mathbf{2_{Dy}}$
Ln–C(η^4-Cb_{cent})/Å	Y1–C1: 2.512(3) Y1–C2: 2.499(3) Y1–C3: 2.466(3) Y1–C4: 2.485(3)	Dy1–C1: 2.519(6) Dy1–C2: 2.503(6) Dy1–C3: 2.473(6) Dy1–C4: 2.485(6)
Ln–(η^4-Cb_{cent})/Å	2.2590(16)	2.264(3)
K–C(η^4-Cb_{cent})/Å	2.7319(17)	2.730(3)
Ln–(η^4-Cb_{cent})–K/°	176.76(8)	176.46(13)

Magnetic property measurements

Magnetic measurements were recorded on a Quantum Design MPMS-XL7 SQUID magnetometer equipped with a 7 T magnet. The samples were restrained in eicosane and sealed in 7 mm NMR tubes. Direct current (DC) magnetic susceptibility measurements were performed on a polycrystalline sample of $\mathbf{1_{Dy}}$ (10.7 mg) and $\mathbf{2_{Dy}}$ (25.0 mg) in the temperature range 1.9-300 K and using an applied field of 1000 Oe. AC susceptibility measurements were performed in zero DC field. Diamagnetic corrections were made using Pascal's constants for all the constituent atoms.[8]

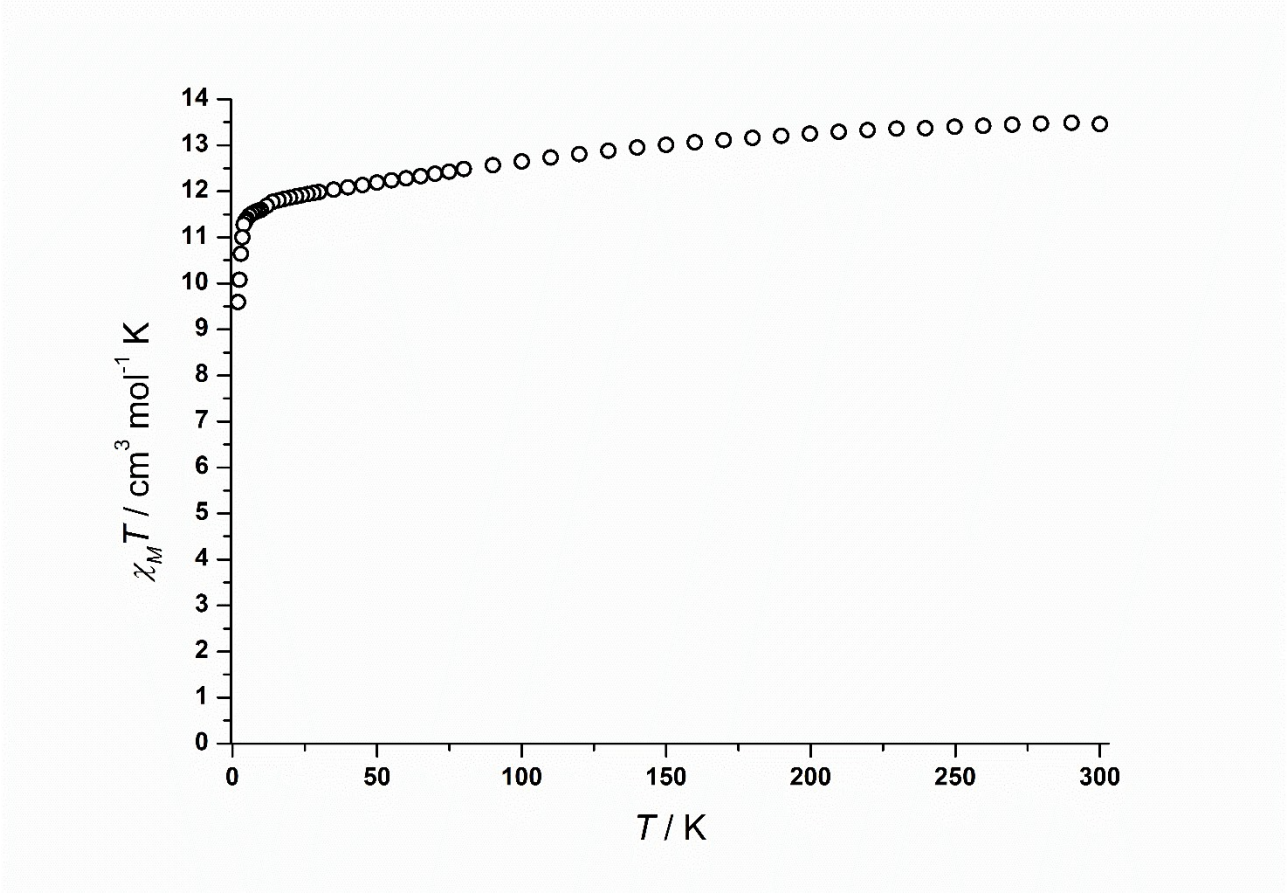

Figure S15. $\chi_M T(T)$ for $\mathbf{1_{Dy}}$ in an applied field of 1000 Oe. $\chi_M T$ (300 K) = 13.46 cm^3 K mol^{-1}, $\chi_M T$ (2 K) = 9.60 cm^3 K mol^{-1}.

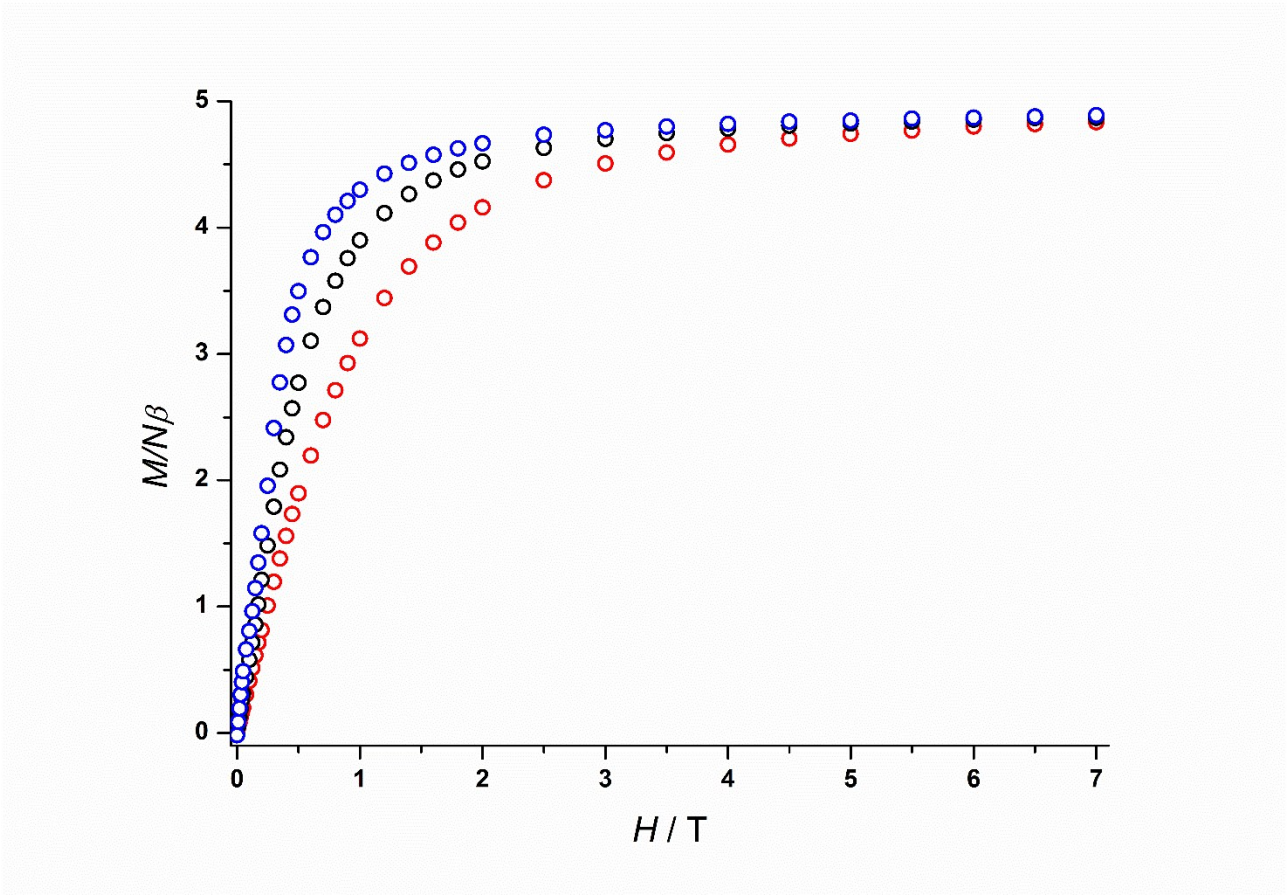

Figure S16. Field (*H*) dependence of the magnetization (*M*) at 1.9 K (blue circles), 3.0 K (black circles) and 5.0 K (red circles) for $\mathbf{1}_{Dy}$. *M* = 4.89 *N*β at 1.9 K and 7 T.

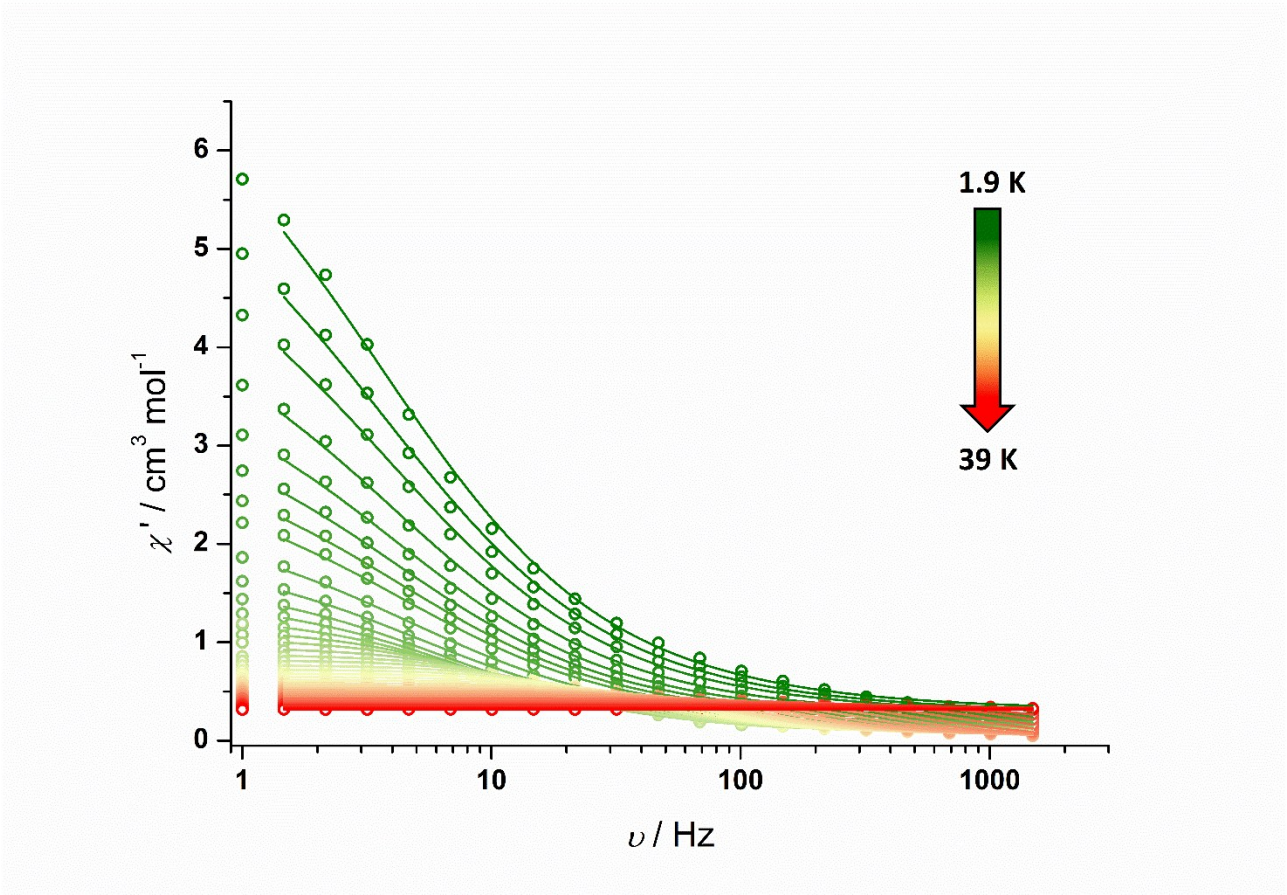

Figure S17. Frequency dependence of the in-phase susceptibility (χ') for $\mathbf{1}_{Dy}$ in zero DC field at ν = 1-1488 Hz and temperatures of 1.9-39 K. Solid lines represent fits to the data using equation 1. The lowest-frequency (1 Hz) data points were not included in the fit due an outlier at 13 K (see S21).

$$\chi'(\nu_{ac}) = \chi_{\infty} + \frac{(\chi_s - \chi_{\infty})[1 + (2\pi\nu_{ac}\tau)^{1-\alpha}\sin(\alpha\pi/2)]}{1 + 2(2\pi\nu_{ac}\tau)^{1-\alpha}\sin(\alpha\pi/2) + (2\pi\nu_{ac}\tau)^{2(1-\alpha)}} \qquad \text{Equation 1}$$

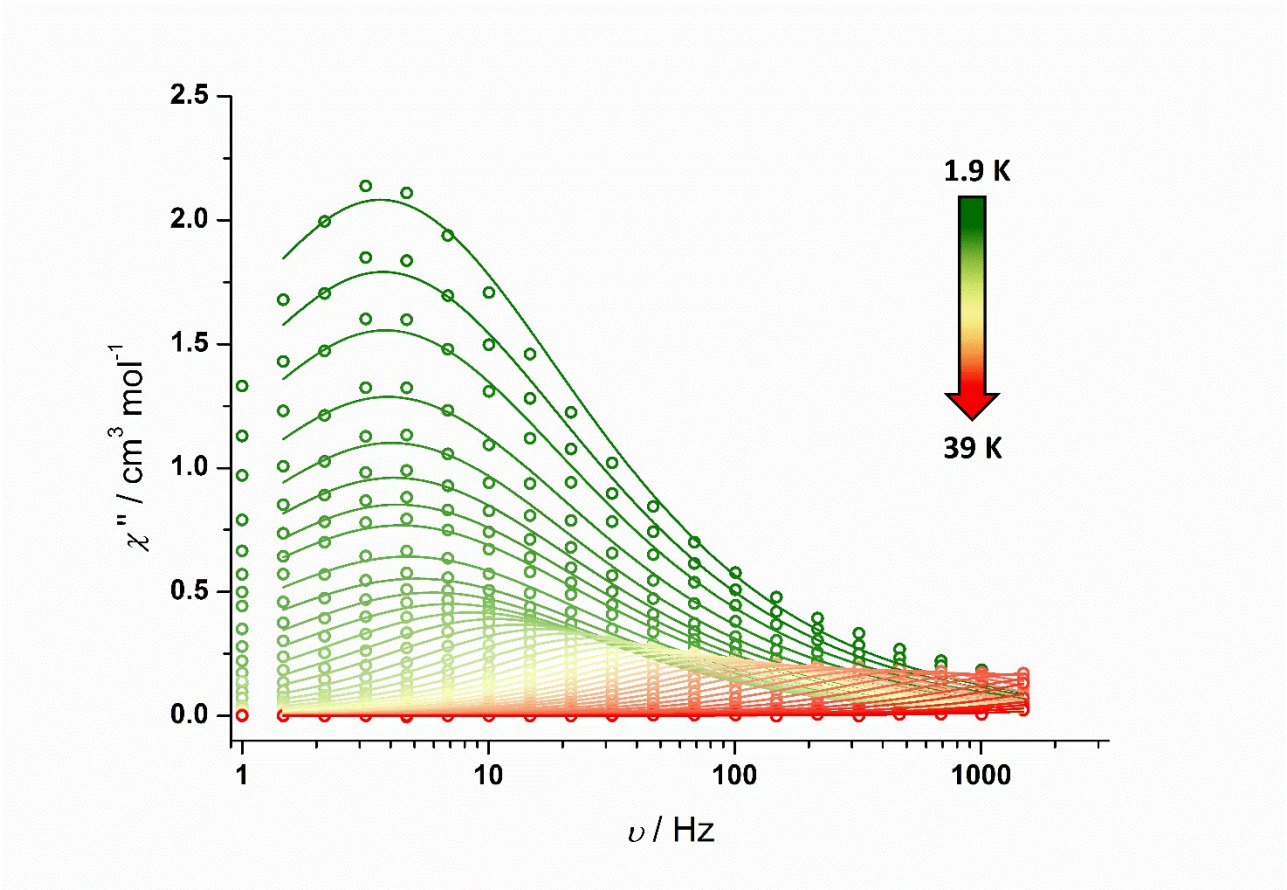

Figure S18. Frequency dependence of the out-of-phase susceptibility (χ'') for $\mathbf{1}_{\mathbf{Dy}}$ in zero DC field at ν= 1-1488 Hz and temperatures of 1.9 to 39 K. Solid lines represent fits to the data using equation 2. The lowest-frequency (1 Hz) data points were not included in the fit due an outlier at 13 K (see S21).

$$\chi''(\nu_{ac}) = \frac{(\chi_s - \chi_\infty)(2\pi\nu_{ac}\tau)^{1-\alpha}\cos(\alpha\pi/2)}{1+2(2\pi\nu_{ac}\tau)^{1-\alpha}\sin(\alpha\pi/2)+(2\pi\nu_{ac}\tau)^{2(1-\alpha)}} \qquad \text{Equation 2}$$

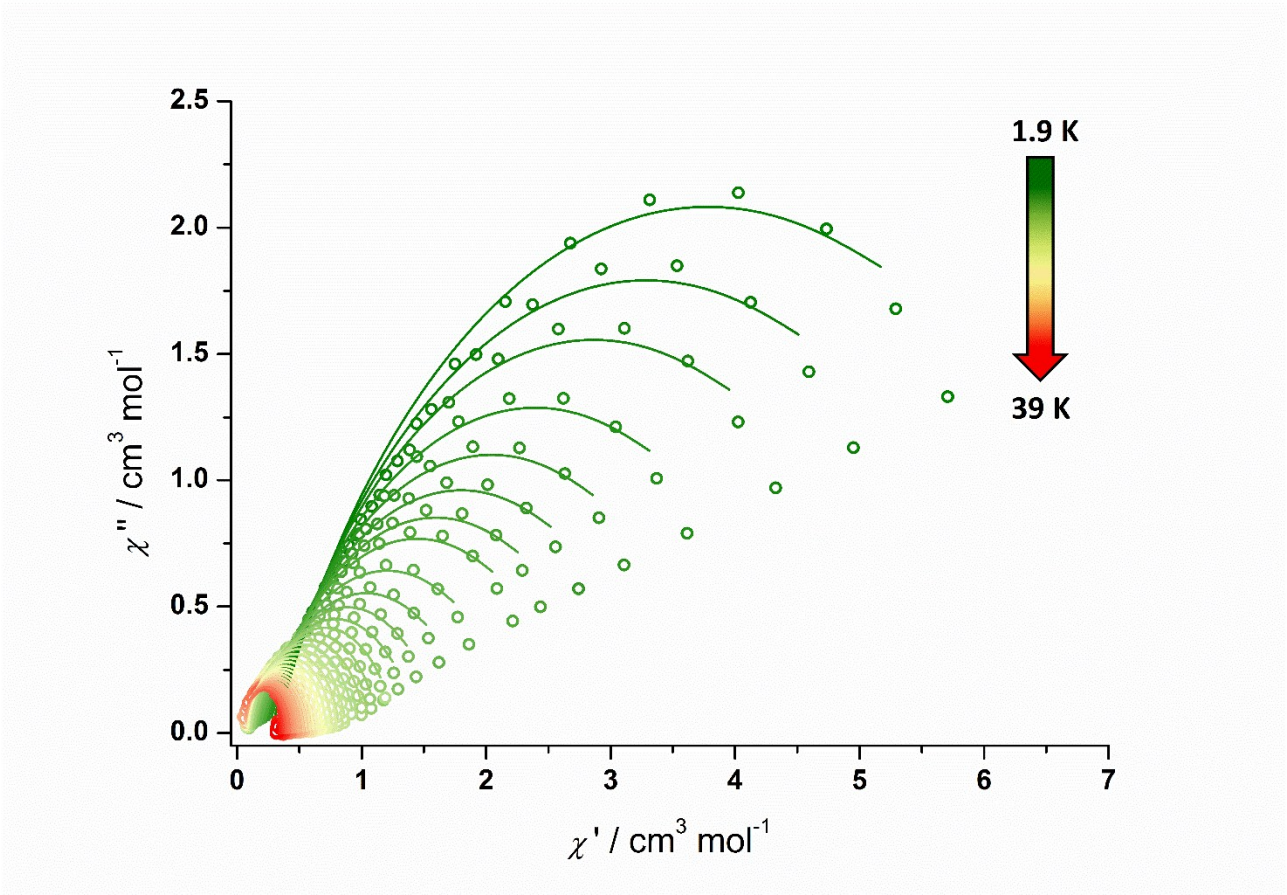

Figure S19. Cole-Cole plots for the AC susceptibilities in zero DC field for $\mathbf{1}_{Dy}$ from 1.9-39 K. Solid lines represent fits to the data using equations 1 and 2. The lowest-frequency (1 Hz) data points were not included in the fit due an outlier at 13 K (see S21).

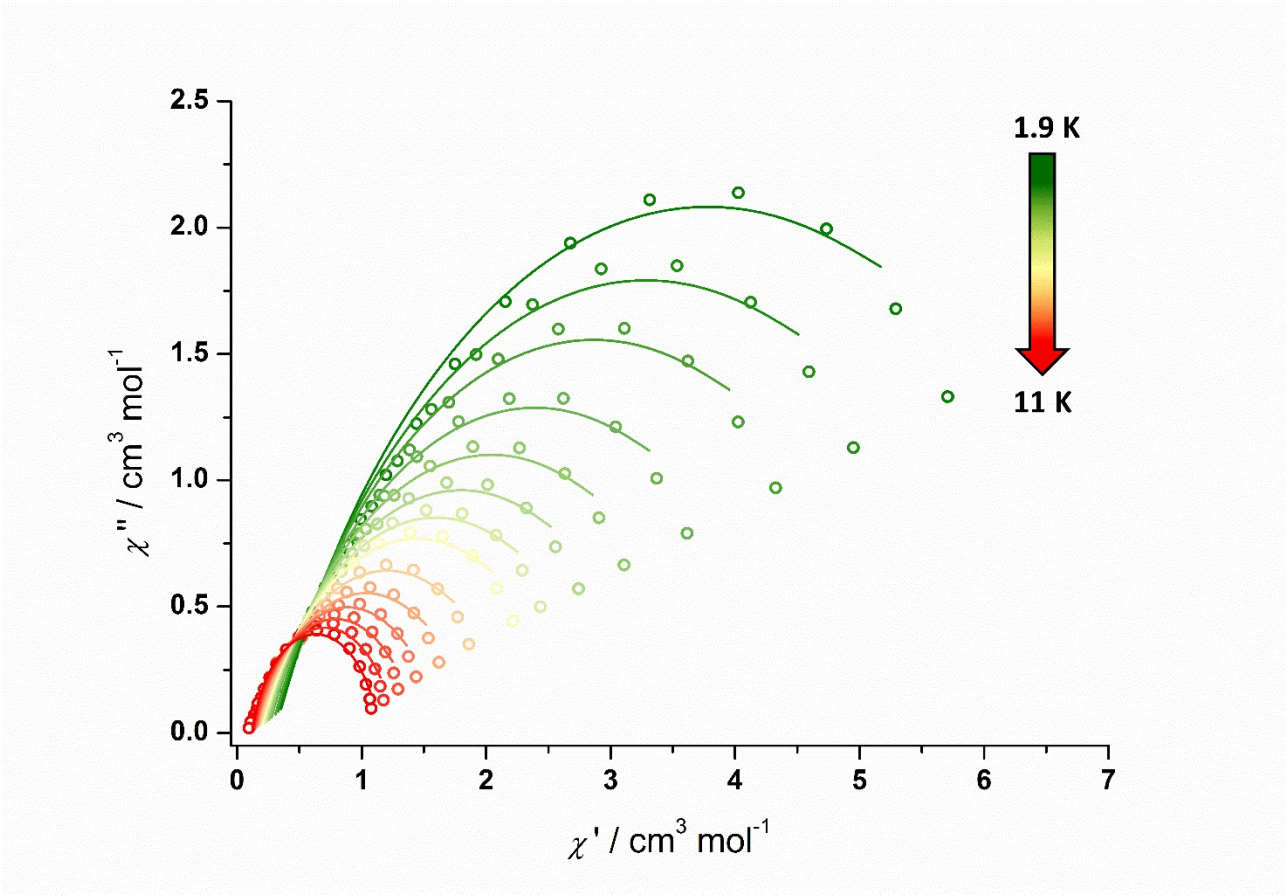

Figure S20. Cole-Cole plots for the AC susceptibilities in zero DC field for $\mathbf{1}_{Dy}$ from 1.9-11 K. Solid lines represent fits to the data using equations 1 and 2. The lowest-frequency (1 Hz) data points were not included in the fit due an outlier at 13 K (see S21).

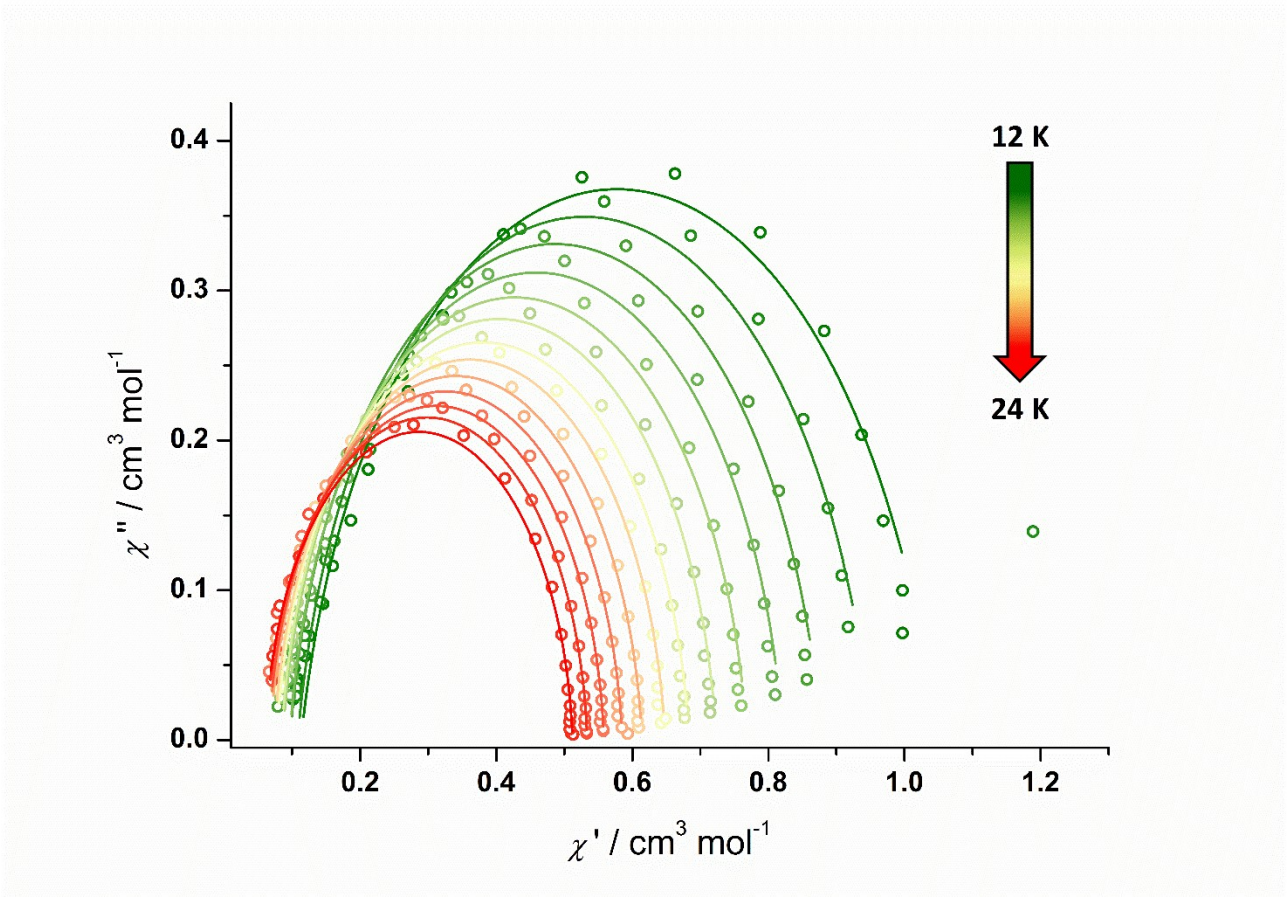

Figure S21. Cole-Cole plots for the AC susceptibilities in zero DC field for $\mathbf{1}_{Dy}$ from 12-24 K. Solid lines represent fits to the data using equations 1 and 2. The lowest-frequency (1 Hz) data points were not included in the fit due an outlier at 13 K.

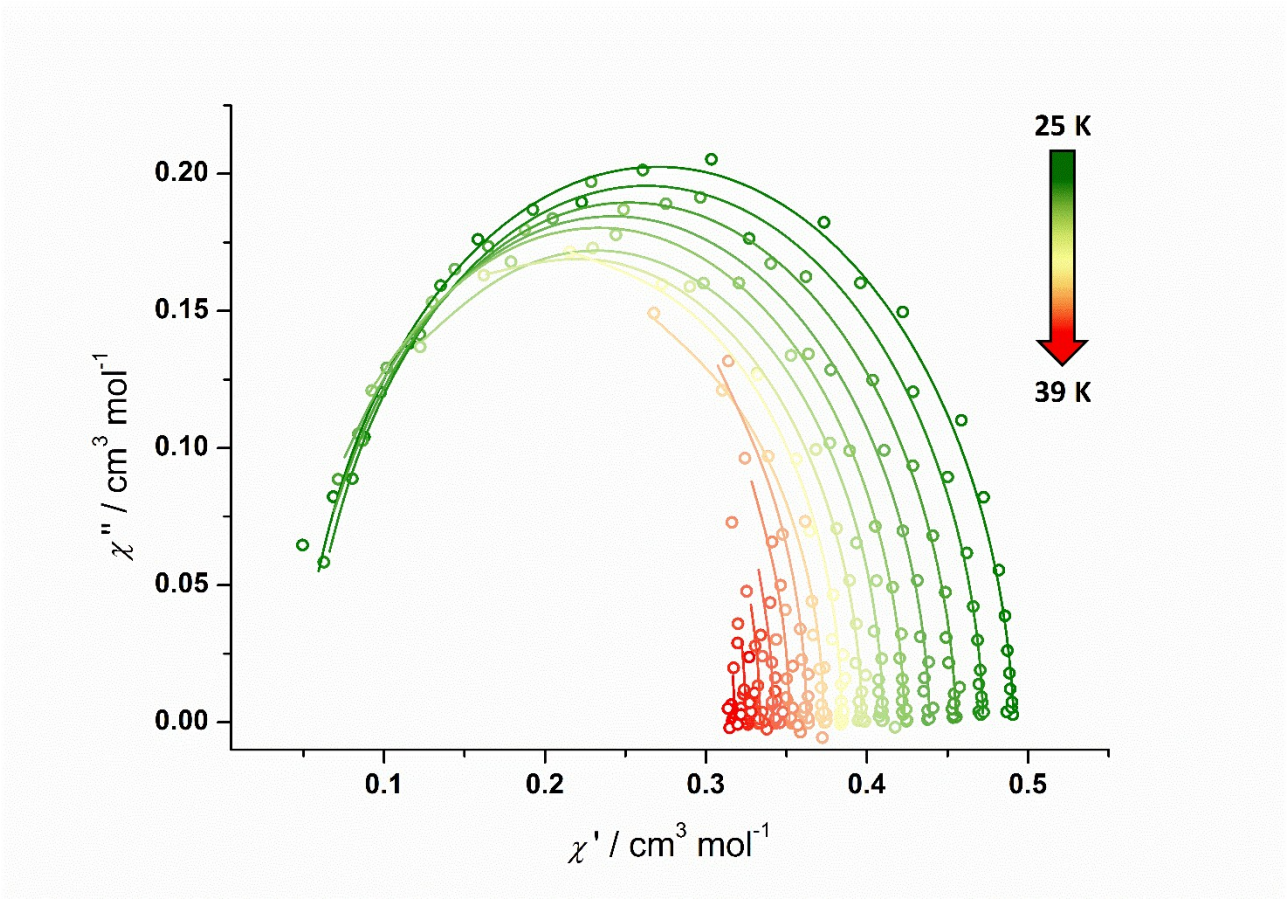

Figure S22. Cole-Cole plots for the AC susceptibilities in zero DC field for $\mathbf{1}_{Dy}$ from 25-39 K. Solid lines represent fits to the data using equations 1 and 2. The lowest-frequency (1 Hz) data points were not included in the fit due an outlier at 13 K (see S21).

Table S4. Relaxation fitting parameters for $\mathbf{1_{Dy}}$ corresponding to Figures S19-22.

T / K	χ_T / cm^3 mol^{-1}	χ_S / cm^3 mol^{-1}	α	τ / s
1.9	7.26107	0.30207	0.30902	0.04387
2.2	6.28936	0.28112	0.31106	0.04273
2.5	5.46138	0.26881	0.30823	0.04176
3	4.54540	0.24193	0.30922	0.04079
3.5	3.86001	0.22912	0.30120	0.03935
4	3.38374	0.21128	0.30242	0.03858
4.5	2.99540	0.19885	0.29871	0.03730
5	2.70321	0.18636	0.29758	0.03642
6	2.24430	0.16756	0.29045	0.03389
7	1.91107	0.15156	0.28065	0.03093
8	1.63086	0.14472	0.24378	0.02664
9	1.44204	0.13431	0.22530	0.02272
10	1.27504	0.12817	0.19294	0.01860
11	1.14273	0.12060	0.16115	0.01490
12	1.04326	0.11270	0.13948	0.01195
13	0.94965	0.10814	0.10768	0.00953
14	0.87670	0.09710	0.09263	0.00763
15	0.82133	0.09625	0.08406	0.00622
16	0.76860	0.08614	0.08007	0.00498
17	0.72313	0.08439	0.06938	0.00413
18	0.68347	0.07701	0.07311	0.00338
19	0.64816	0.07357	0.06645	0.00281
20	0.61420	0.06792	0.06227	0.00233
21	0.58512	0.06562	0.05725	0.00197
22	0.55834	0.06514	0.05112	0.00166
23	0.53367	0.06161	0.04547	0.00138
24	0.51195	0.06046	0.04628	0.00112
25	0.49122	0.04848	0.04364	0.00091
26	0.47217	0.05363	0.02951	0.00073
27	0.45525	0.04989	0.02915	0.00056
28	0.43907	0.04520	0.02798	0.00041
29	0.42342	0.04283	0.02039	0.00030
30	0.40998	0.05437	0.00664	0.00022
31	0.39692	0.04448	0.01247	0.00015
32	0.38435	0.04132	0.00000	0.00011
33	0.37303	0.06053	0.00000	0.00008
34	0.36239	0.00000	0.00000	0.00005
35	0.35179	0.00000	0.00000	0.00003
36	0.34198	0.00000	0.00000	0.00002
37	0.33352	0.00000	0.00000	0.00001
38	0.32470	0.00000	0.00000	0.00001
39	0.31767	0.00000	0.00000	0.00001

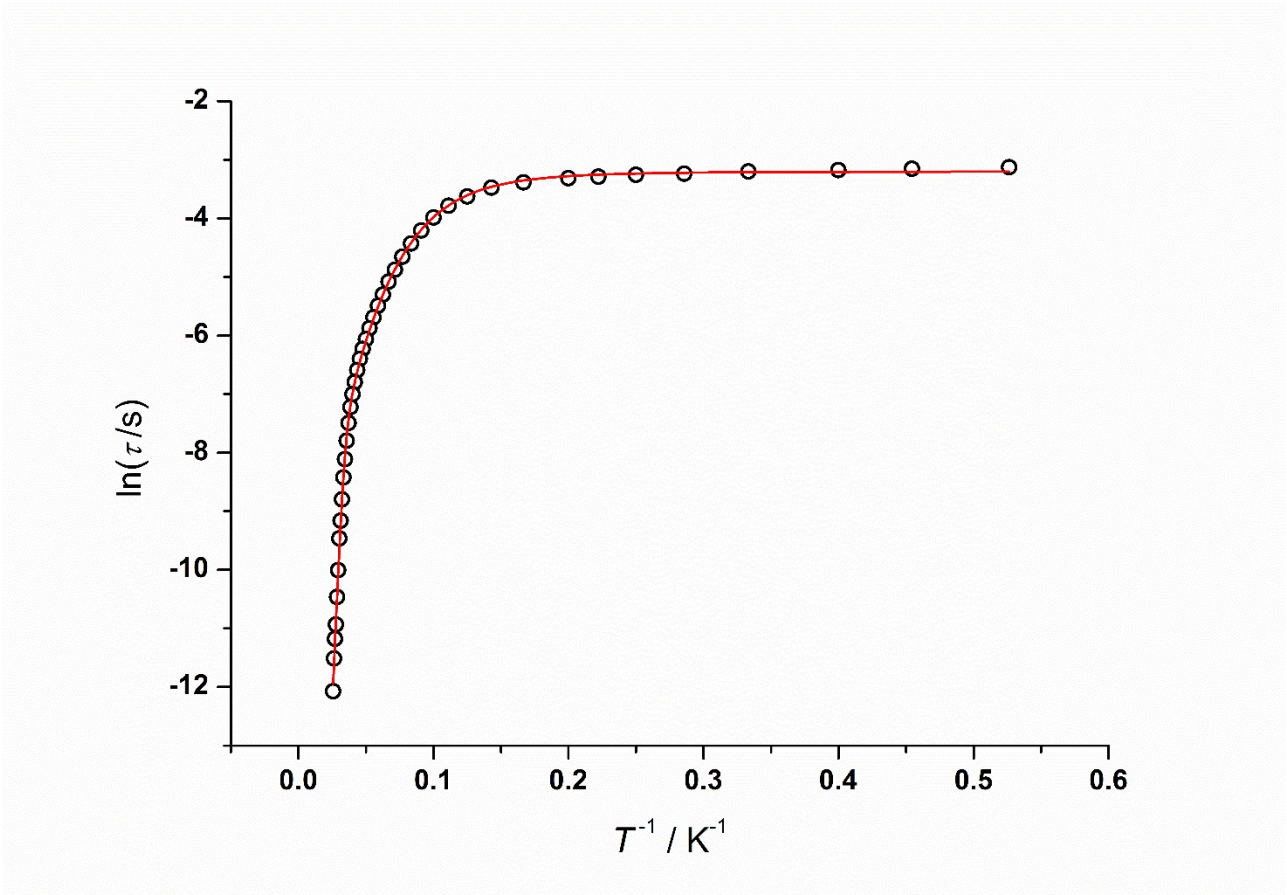

Figure S23. Plot of natural log of the relaxation time (τ) *vs.* inverse temperature for $\mathbf{1}_{\mathbf{Dy}}$. The black points are from the AC susceptibility measurements. The solid red line is the best fit (adjusted R^2 = 0.99962) to $\tau^{-1} = \tau_0^{-1} e^{-U_{eff}/k_B T} + CT^n + \tau_{QTM}^{-1}$, giving: U_{eff} = 371(7) cm^{-1} (or 534(10) K), τ_0 = 7.8(2) × 10^{-12} s, C = 0.0041(7) s^{-1} K^{-n}, n = 3.85(6) and τ_{QTM} = 0.041(1) s.

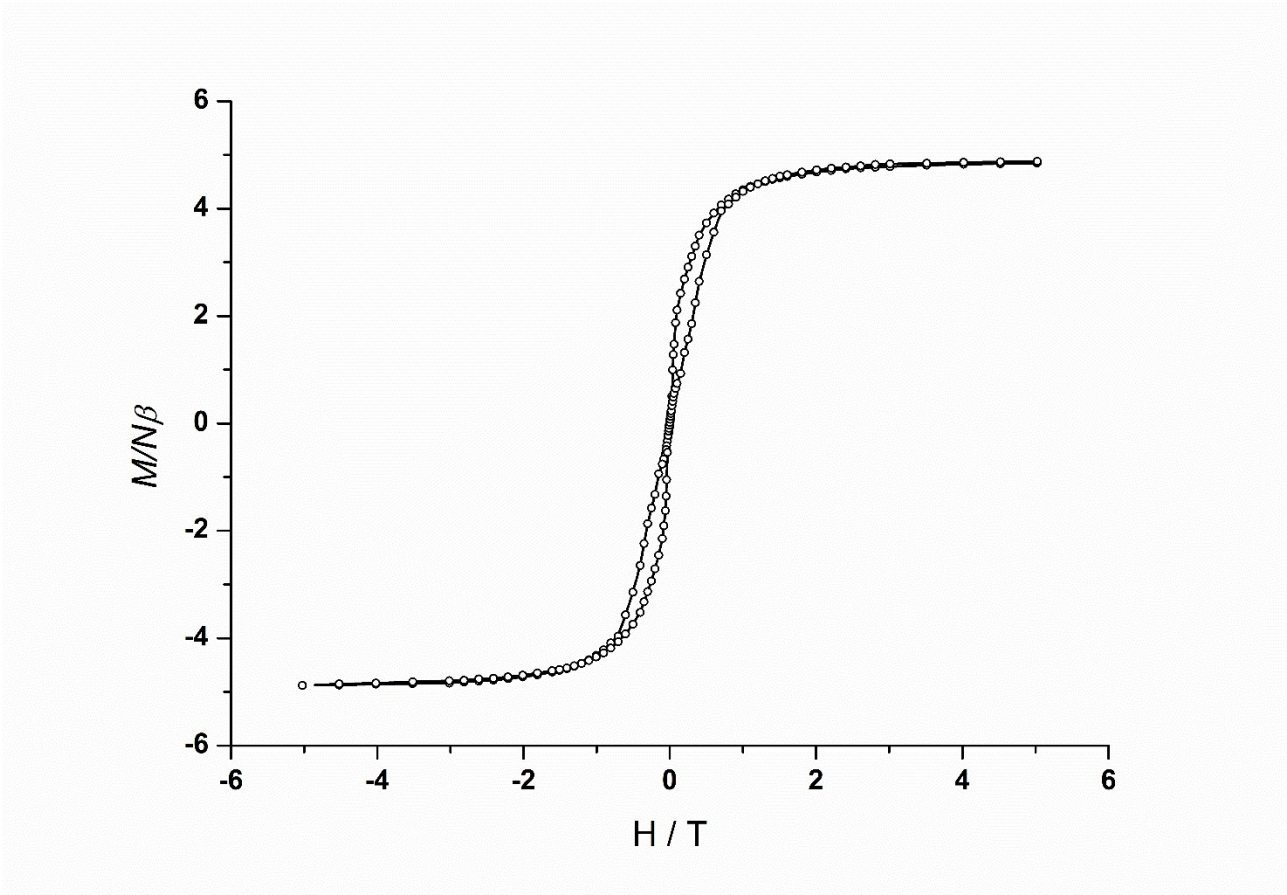

Figure S24. Magnetic hysteresis loops for $\mathbf{1}_{Dy}$. The data were continuously collected at 1.9 K under a varying field sweep rate (1.1 mT s^{-1} |0-1| T, 3.0 mT s^{-1} |1-2| T, 4.5 mT s^{-1} |2-3| T and 8.5 mT s^{-1} |3-5| T). Solid lines are a guide to the eye.

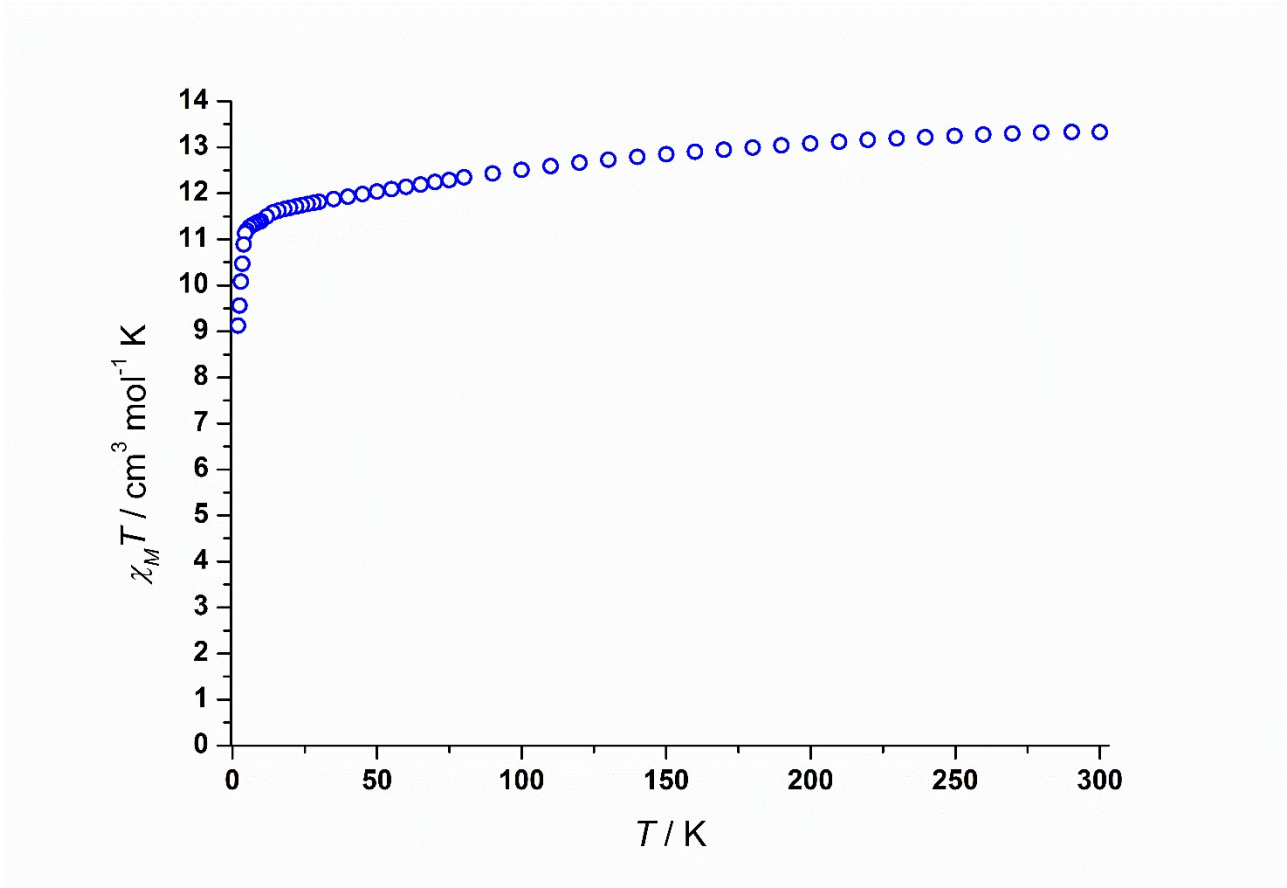

Figure S25. Plot of $\chi_M T(T)$ for $\mathbf{2_{Dy}}$ in an applied field of 1000 Oe. $\chi_M T$(300 K) = 13.52 cm^3 K mol^{-1}, $\chi_M T$(2 K) = 9.13 cm^3 K mol^{-1}.

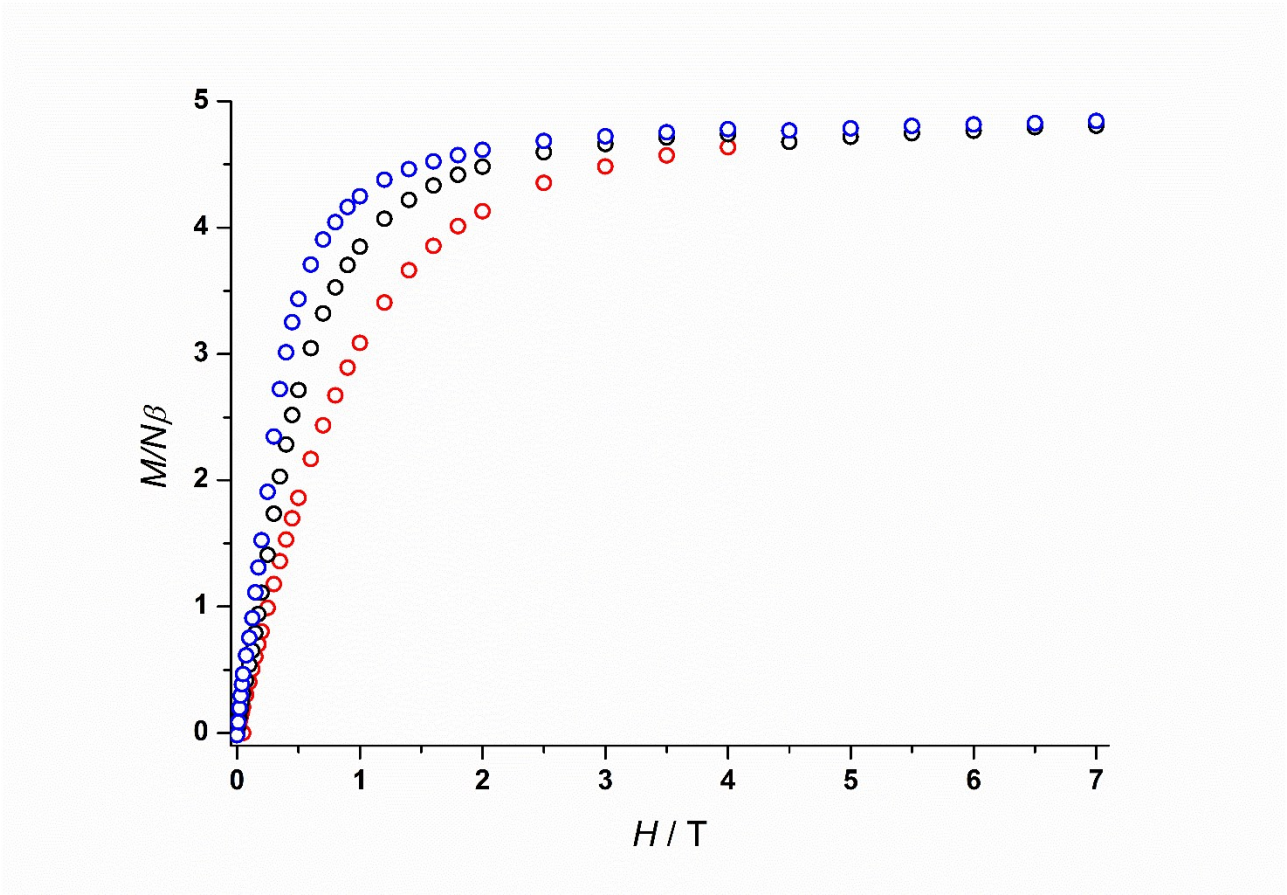

Figure S26. Field (*H*) dependence of the magnetization (*M*) at 1.9 K (blue circles), 3.0 K (black circles) and 5.0 K (red circles) for $\mathbf{2_{Dy}}$. *M* = 4.85 *N*β at 1.9 K and 7 T.

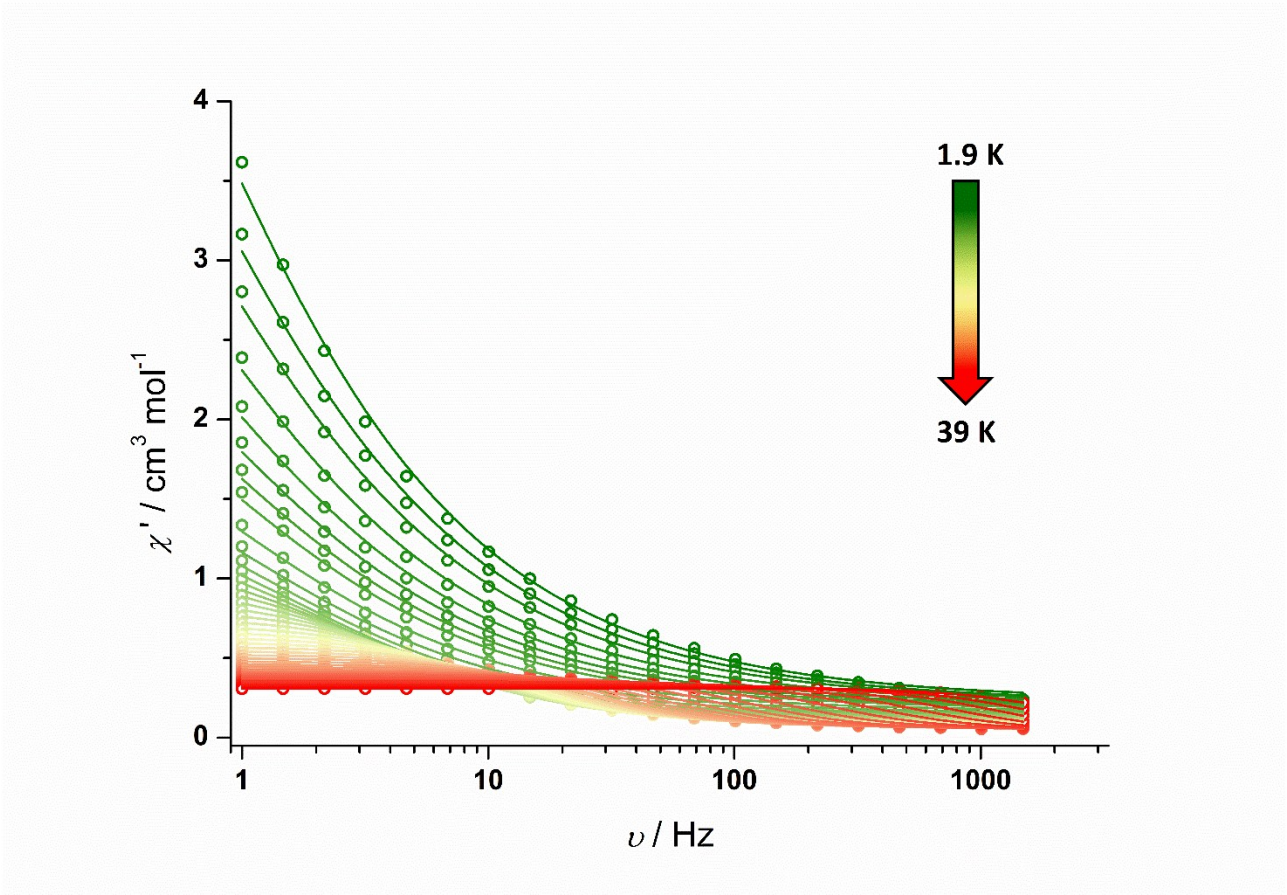

Figure S27. Frequency dependence of the in-phase susceptibility (χ') for $\mathbf{2_{Dy}}$ in zero DC field at AC frequencies of ν = 1-1488 Hz and temperatures of 1.9-39 K. Solid lines represent fits to the data using equation 1, which describes χ' in terms of ν, isothermal susceptibility (χ_T), adiabatic susceptibility (χ_S), relaxation time (τ), and a variable representing the distribution of relaxation times (α).

$$\chi'(\nu_{ac}) = \chi_{\infty} + \frac{(\chi_s - \chi_{\infty})[1 + (2\pi\nu_{ac}\tau)^{1-\alpha}\sin(\alpha\pi/2)]}{1 + 2(2\pi\nu_{ac}\tau)^{1-\alpha}\sin(\alpha\pi/2) + (2\pi\nu_{ac}\tau)^{2(1-\alpha)}} \qquad \text{Equation 1}$$

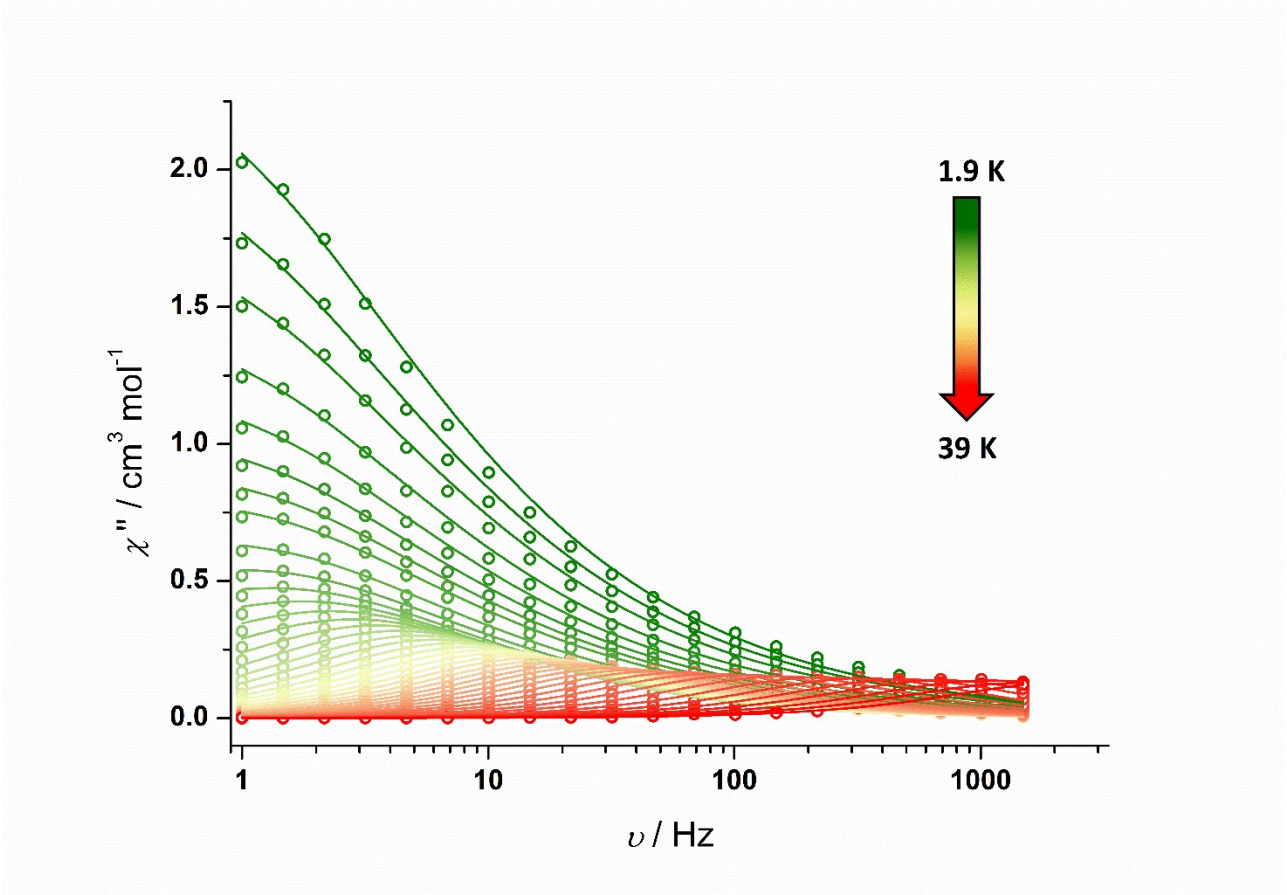

Figure S28. Frequency dependence of the out-of-phase susceptibility (χ'') for $\mathbf{2_{Dy}}$ in zero DC field at AC frequencies of ν = 1-1488 Hz and temperatures of 1.9-39 K. Solid lines represent fits to the data using equation 2, which describes χ'' in terms of frequency, isothermal susceptibility (χ_T), adiabatic susceptibility (χ_S), relaxation time (τ), and a variable representing the distribution of relaxation times (α).

$$\chi''(\nu_{ac}) = \frac{(\chi_s - \chi_\infty)(2\pi\nu_{ac}\tau)^{1-\alpha}\cos(\alpha\pi/2)}{1+2(2\pi\nu_{ac}\tau)^{1-\alpha}\sin(\alpha\pi/2)+(2\pi\nu_{ac}\tau)^{2(1-\alpha)}} \qquad \text{Equation 2}$$

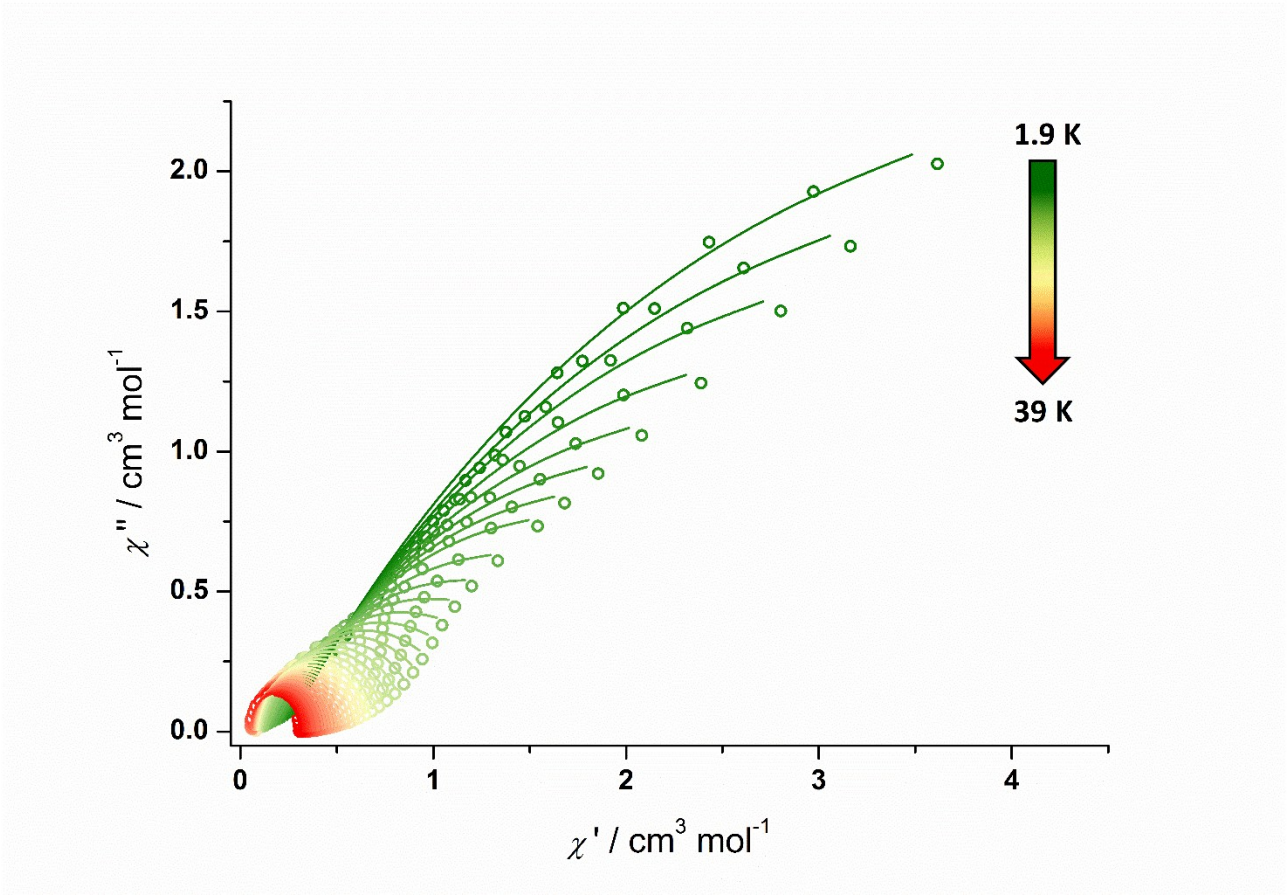

Figure S29. Cole-Cole plots for the AC susceptibilities in zero DC field for $\mathbf{2_{Dy}}$ from 1.9-39 K. Solid lines represent fits to the data using equations 1 and 2.

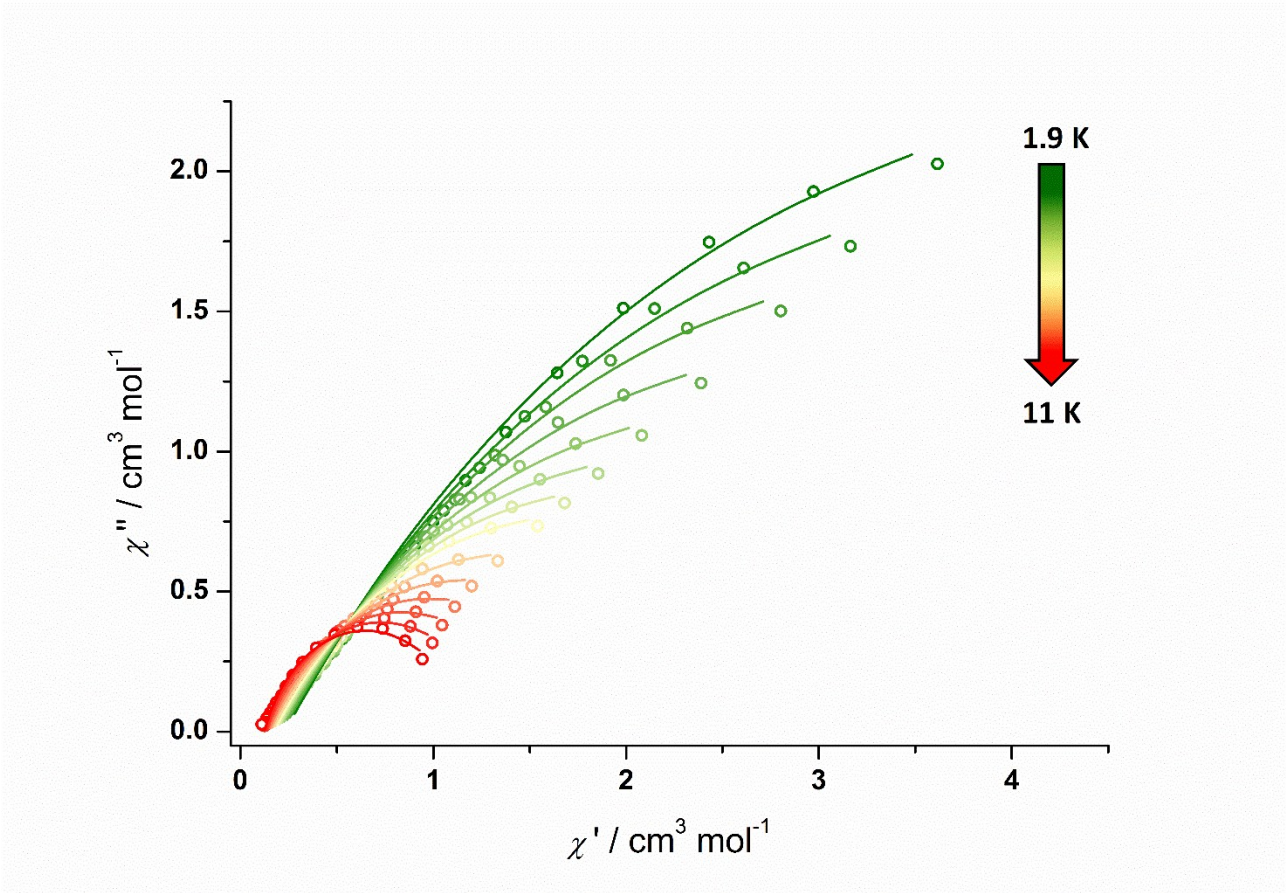

Figure S30. Cole-Cole plots for the AC susceptibilities in zero DC field for $\mathbf{2_{Dy}}$ from 1.9-11 K. Solid lines represent fits to the data using equations 1 and 2.

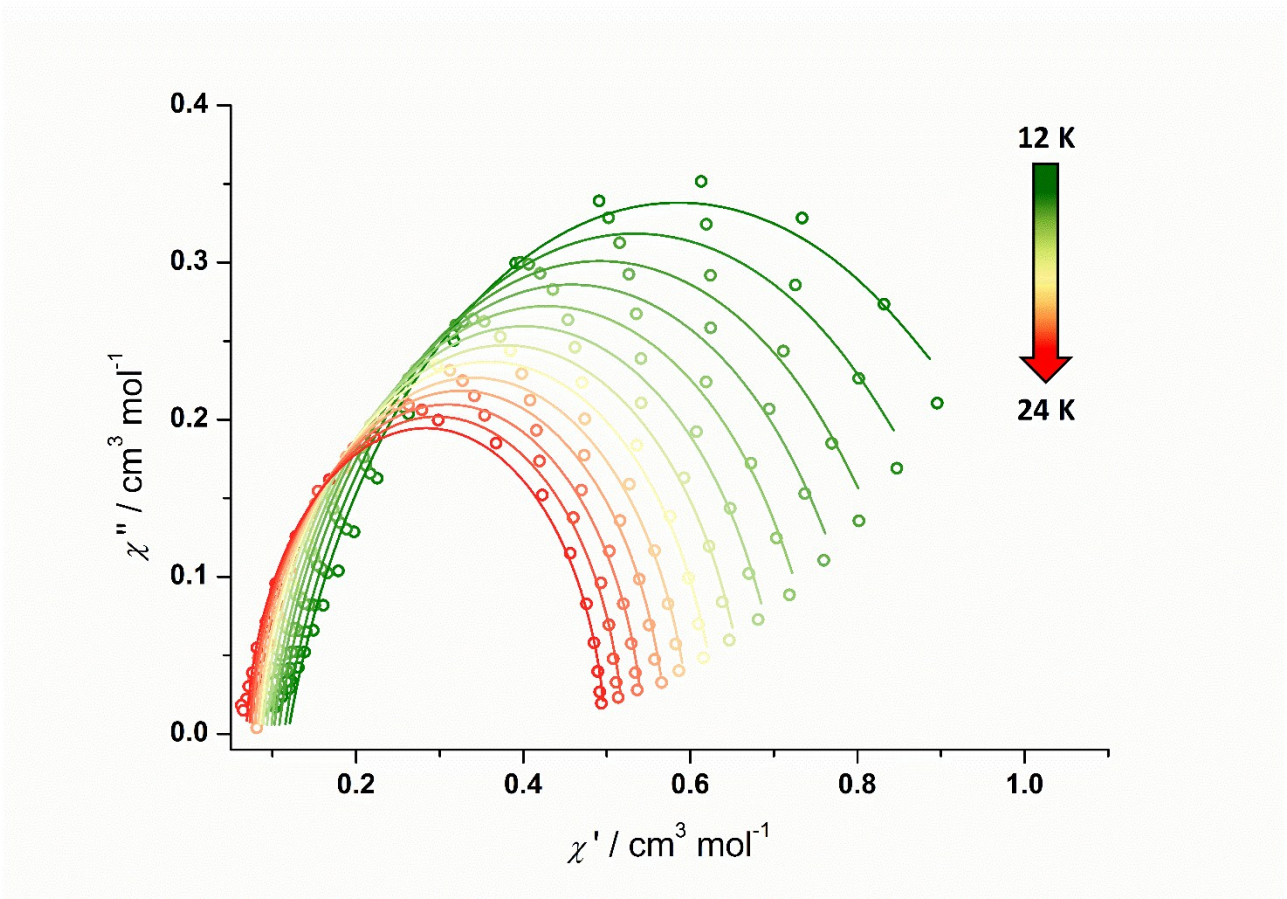

Figure S31. Cole-Cole plots for the AC susceptibilities in zero DC field for $\mathbf{2_{Dy}}$ from 12-24 K. Solid lines represent fits to the data using equations 1 and 2.

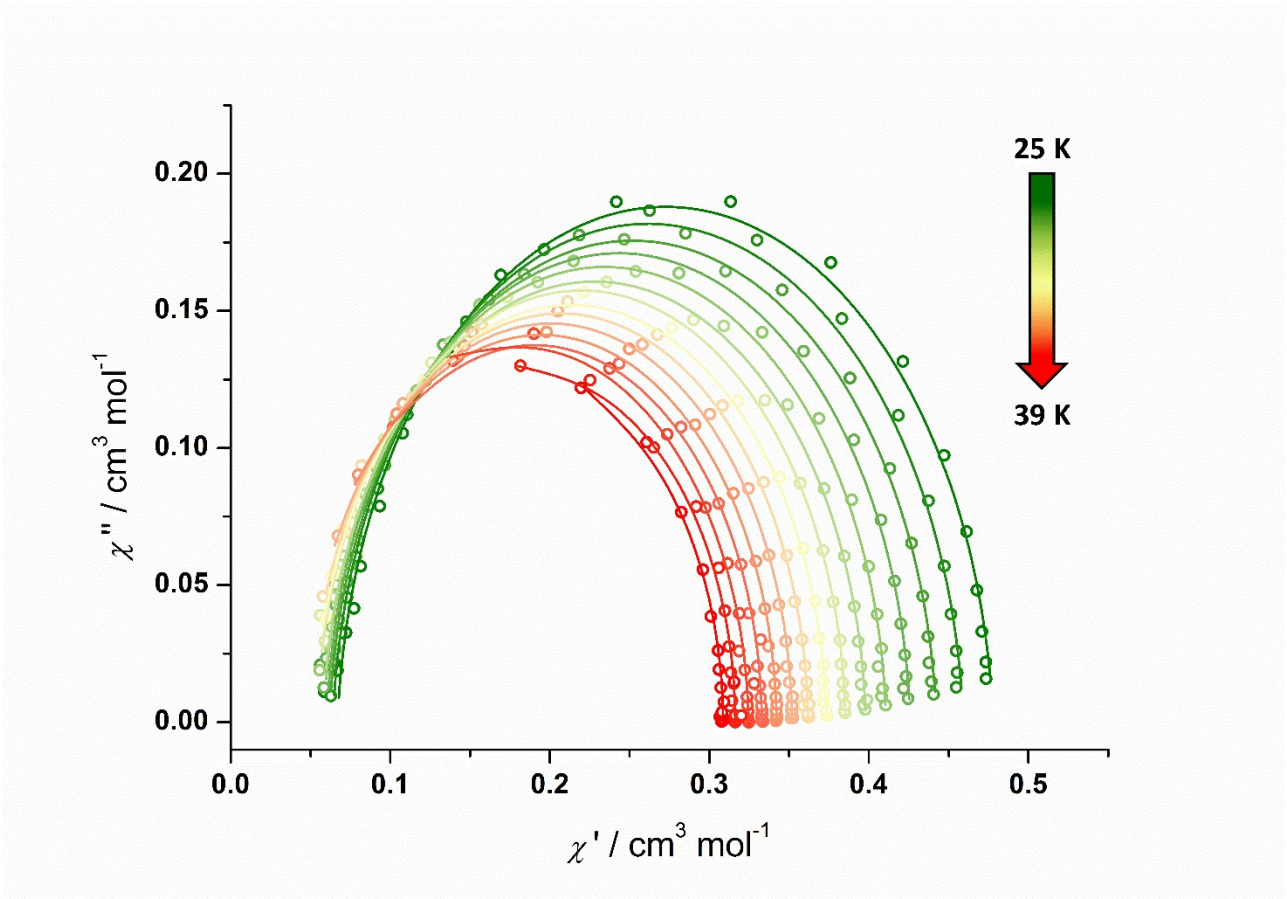

Figure S32. Cole-Cole plots for the AC susceptibilities in zero DC field for $\mathbf{2}_{Dy}$ from 25-39 K. Solid lines represent fits to the data using equations 1 and 2.

Table S4. Relaxation fitting parameters for $\mathbf{2_{Dy}}$ corresponding to Figures S29-32.

T / K	χ_T / cm^3 mol^{-1}	χ_S / cm^3 mol^{-1}	α	τ / s
1.9	9.16763	0.23175	0.41935	0.34616
2.2	8.02566	0.21819	0.42749	0.35221
2.5	6.88190	0.21616	0.42426	0.32825
3	5.63352	0.20883	0.42033	0.30172
3.5	4.74741	0.19856	0.41710	0.28003
4	4.08750	0.19029	0.41219	0.25859
4.5	3.57429	0.18282	0.40629	0.23816
5	3.17964	0.17446	0.40118	0.22052
6	2.57348	0.16168	0.38569	0.18544
7	2.13048	0.15128	0.36297	0.15016
8	1.79036	0.14424	0.33126	0.11732
9	1.52737	0.13706	0.29587	0.09038
10	1.32470	0.13219	0.25739	0.07017
11	1.17338	0.12454	0.22739	0.05588
12	1.05268	0.11851	0.19519	0.04495
13	0.95419	0.11373	0.16640	0.03678
14	0.87678	0.10679	0.14661	0.03050
15	0.81485	0.10115	0.13058	0.02581
16	0.75810	0.09794	0.11204	0.02187
17	0.71025	0.09249	0.10013	0.01860
18	0.66882	0.08790	0.09101	0.01596
19	0.63263	0.08423	0.08190	0.01380
20	0.59962	0.08189	0.07281	0.01196
21	0.57124	0.07836	0.06501	0.01044
22	0.54425	0.07444	0.06003	0.00905
23	0.52016	0.07212	0.05368	0.00790
24	0.49829	0.06855	0.05036	0.00675
25	0.47781	0.06690	0.04365	0.00586
26	0.45908	0.06390	0.04007	0.00491
27	0.44246	0.06168	0.03818	0.00408
28	0.42587	0.06020	0.02893	0.00330
29	0.41080	0.05851	0.02385	0.00258
30	0.39801	0.05795	0.02209	0.00196
31	0.38537	0.05425	0.01791	0.00143
32	0.37351	0.05301	0.01946	0.00101
33	0.36186	0.05148	0.01138	0.00070
34	0.35180	0.04949	0.01040	0.00048
35	0.34218	0.04722	0.01327	0.00033
36	0.33288	0.04845	0.00706	0.00023
37	0.32462	0.03663	0.01892	0.00015
38	0.31620	0.05470	0.00286	0.00011
39	0.30864	0.04725	0.00554	0.00008

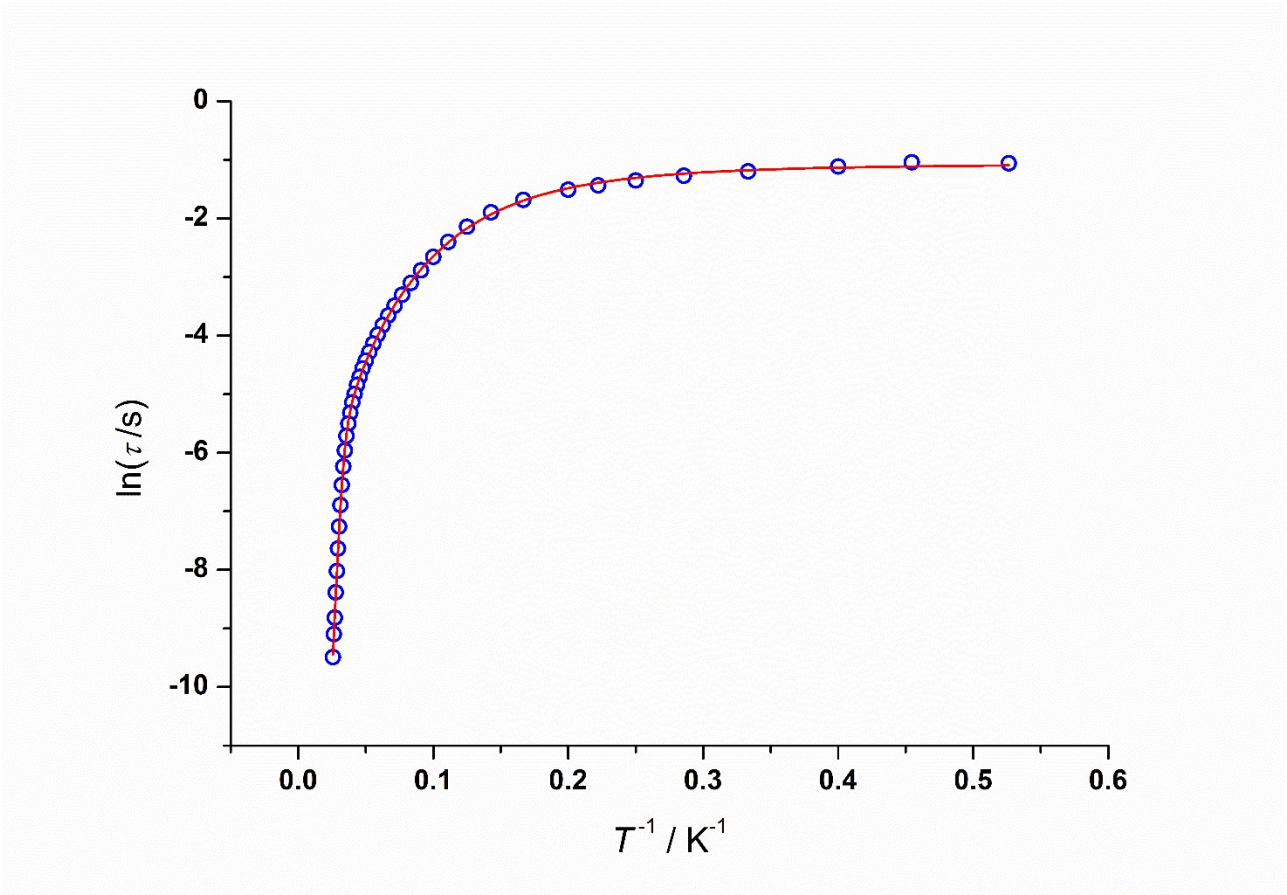

Figure S33. Plot of natural log of the relaxation time (τ) *vs.* inverse temperature for $\mathbf{2_{Dy}}$. The blue points are from the AC susceptibility measurements. The solid red line is the best fit (adjusted R^2 = 0.99985) to $\tau^{-1} = \tau_0^{-1} e^{-U_{eff}/k_B T} + CT^n + \tau_{QTM}^{-1}$, giving: U_{eff} = 357(4) cm^{-1} (or 513(6) K), τ_0 = 1.8(3) × 10^{-10} s, C = 0.014(2) s^{-1} K^{-n}, n = 2.90(4) and τ_{QTM} = 0.36(3) s.

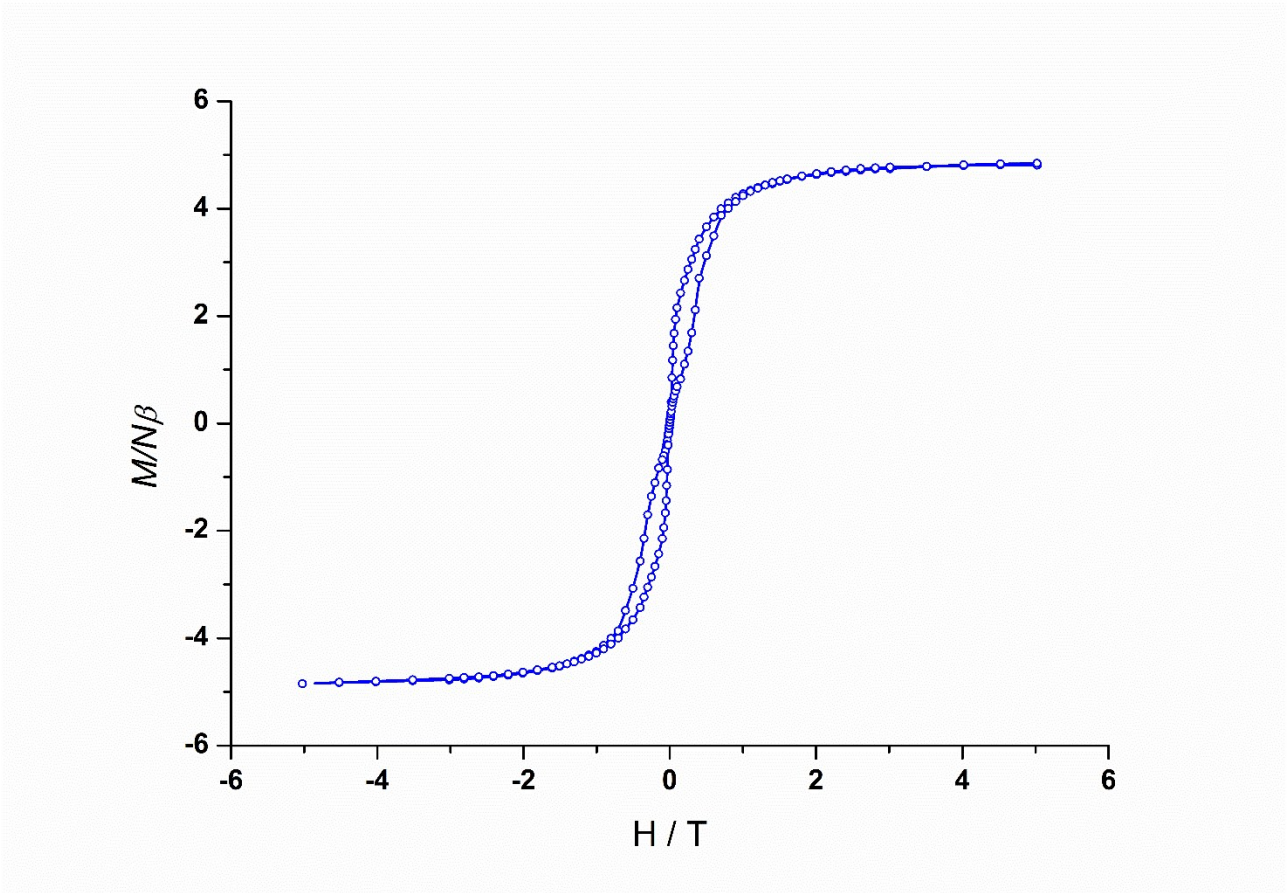

Figure S34. Magnetic hysteresis loops for $\mathbf{2}_{Dy}$. The data were continuously collected at 1.9 K under a varying field sweep rate (1.1 mT s^{-1} |0-1| T, 3.0 mT s^{-1} |1-2| T, 4.5 mT s^{-1} |2-3| T and 8.5 mT s^{-1} |3-5| T). Solid lines are a guide to the eye.

Computational Details

The DFT optimization of the hydrogen atom positions was carried out using the *Gaussian 09* quantum chemistry software revision E.01[9] and the hybrid PBE0 exchange-correlation (XC) functional[10]. The basis set used for the Dy^{3+} ion consisted of a 4*f*-in-core MWB55 effective core potential (ECP) along with a corresponding valence basis set.[11] Ahlrichs' valence-polarized triple-ζ basis (TZVP)[12] was used for other atoms. The quality of the integration grid was set to "UltraFine" in Gaussian and the accuracy of two-electron integrals was raised to 10^{-12} atomic units.

The multireference calculations were carried out using the *OpenMolcas* quantum chemistry software version 19.11.[13] Roos' relativistically contracted atomic natural orbital (ANO-RCC) basis sets were used throughout.[14] A polarized valence-quadruple-ζ (VQZP) quality basis was used for the Dy^{3+} ion. In the central {(Cb'''')Dy$(BH_4)_2$(THF)} unit, polarized valence-triple-ζ (VTZP) bases were used for the $[BH_4]^-$ ions, the C atoms in the coordinated THF and the Cb ring as well as the K^+ ions. Polarized valence-double-ζ (VDZP) bases were used for the remaining fragments in the central {(Cb'''')Dy$(BH_4)_2$(THF)} unit. A valence-double-ζ basis was used for the Y^{3+} ions and a minimal basis (MB) was used for the remaining atoms in the terminal {(Cb'''')Y$(BH_4)_2$(THF)} units. Cholesky decomposition with a threshold of 10^{-8} atomic units was used in storage of the two-electron integrals. Scalar relativistic effects were introduced using the scalar version of the exact two-component (X2C) transformation[15] as implemented in OpenMolcas.

The multieference calculations consisted of a series of state-averaged complete active space self-consistent field (SA-CASSCF) calculations. The active space consisted of the nine 4*f* electrons in the seven 4*f* orbitals. All 21 sextet, 224 quartet and 490 doublet roots were solved in three separate calculations. Spin-orbit coupling was introduced using the well-established the spin-orbit restricted active state interaction (SO-RASSI) approach.[16] The SOC operator was then constructed in the basis of the lowest 21 sextet, 128 quartet and 130 doublet SA-CASSCF eigenstates (corresponding to an energy cut-off of 50,000 cm^{-1}) using the atomic mean-field integral (AMFI) formalism[17] and diagonalized to yield the spin-orbit coupled eigenstates. The static magnetic properties (**g**-tensors, *ab initio* crystal-field parameters and the effective barrier for the relaxation of magnetization) were calculated using the SINGLE_ANISO_OPEN module[18-20] of OpenMolcas.

Table S5. Energies and principal components of the **g**-tensors of the eight lowest Kramers doublets (KDs) of the ground $^6H_{15/2}$ multiplet of $\mathbf{2_{Dy}}$.

	E / cm^{-1}	g_x	g_y	g_z	θ^a
KD1	0	0.000926	0.001305	19.834476	0.0°
KD2	242	0.093017	0.117100	17.079967	169.5°
KD3	326	0.534145	0.561381	14.226165	167.1°
KD4	383	0.008395	0.950690	11.947312	10.7°
KD5	455	2.296561	3.068187	9.469676	21.2°
KD6	540	3.441120	5.710016	9.389138	92.0°
KD7	657	8.141186	5.698843	2.441712	7.3°
KD8	701	11.595478	9.230990	1.146477	1.9°

[a] The angle between the principal magnetic axis of the given doublet and the that of the ground doublet.

Table S6. Transition magnetic moments between various states in the eight lowest KDs of the in $\mathbf{2_{Dy}}$.

Initial KD	Final KD	Transition on the same side of the barrier	Transition on the same side of the barrier
KD1	KD1	3.3057	0.0004
KD2	KD2	3.5341	0.0353
KD3	KD3	3.0179	0.1849
KD4	KD4	2.3354	0.2106
KD5	KD5	2.2264	0.9224
KD6	KD6	1.3073	2.4009
KD7	KD7	0.8998	2.2470
KD8	KD8	1.0008	3.3929
KD1	KD2	1.7216	0.0029
KD2	KD3	2.4080	0.0543
KD3	KD4	2.9182	0.1920
KD4	KD5	3.0462	0.2086
KD5	KD6	3.0339	0.7972
KD6	KD7	2.5446	0.6687
KD7	KD8	3.3316	0.5610
KD1	KD3	0.4082	0.0209
KD2	KD4	0.3287	0.0691
KD3	KD5	0.6150	0.1352
KD4	KD6	0.6450	0.3560
KD5	KD7	0.3770	0.8656
KD6	KD8	0.1642	0.9943
KD1	KD4	0.3391	0.0108
KD2	KD5	0.5794	0.0316
KD3	KD6	0.3279	0.1476
KD4	KD7	0.2120	0.3394
KD5	KD8	0.4243	0.2449
KD1	KD5	0.0976	0.0205
KD2	KD6	0.1422	0.1586
KD3	KD7	0.1696	0.1361
KD4	KD8	0.1204	0.2931
KD1	KD6	0.0770	0.0178
KD2	KD7	0.1703	0.0336
KD3	KD8	0.2768	0.1614
KD1	KD7	0.0288	0.0218
KD2	KD8	0.1531	0.0589
KD1	KD8	0.0268	0.0155

Table S7. *Ab initio* crystal-field parameters B_{kq} (in cm^{-1}) for $\mathbf{2_{Dy}}$ listed in the Iwahara–Chibotaru notation.

k	q	Re(B_{kq})	Im(B_{kq})	$\lvert B_{kq}\rvert$
2	0	–376.668572	0.000000	376.668572
2	1	10.148887	–10.972468	14.946403
2	2	13.212098	–14.032149	19.273316
4	0	3.365113	0.000000	3.365113
4	1	–0.019546	–0.269856	0.270563
4	2	–6.425327	11.427467	13.109989
4	3	–2.604809	29.215574	29.331464
4	4	4.118578	28.888473	29.180585
6	0	–36.637984	0.000000	36.637984
6	1	–4.670457	4.211427	6.288822
6	2	–8.180194	8.934668	12.113788
6	3	0.819490	–4.643460	4.715218
6	4	0.473932	–6.374391	6.391985
6	5	–11.019572	–9.660280	14.654419
6	6	10.504192	1.653741	10.633575
8	0	0.373640	0.000000	0.373640
8	1	0.068580	–0.038346	0.078572
8	2	0.151947	–0.131781	0.201132
8	3	0.002206	0.113874	0.113895
8	4	0.012709	0.195364	0.195777
8	5	0.111084	0.107703	0.154724
8	6	–0.048048	–0.004215	0.048232
8	7	0.011732	–0.004243	0.012476
8	8	0.023321	–0.026911	0.035610
10	0	0.008366	0.000000	0.008366
10	1	0.001941	0.000249	0.001957
10	2	–0.004284	–0.002800	0.005118
10	3	–0.005126	–0.015152	0.015995
10	4	–0.004848	–0.009302	0.010489
10	5	0.007978	0.007734	0.011112
10	6	0.001320	0.000509	0.001415
10	7	0.011056	0.000711	0.011079
10	8	0.007886	–0.004500	0.009080
10	9	0.006036	–0.005363	0.008075
10	10	–0.000211	0.006376	0.006379

12	0	0.004428	0.000000	0.004428
12	1	–0.000190	–0.000996	0.001014
12	2	0.002124	–0.002837	0.003544
12	3	0.000258	0.001064	0.001095
12	4	–0.000019	–0.000104	0.000106
12	5	0.001232	0.000743	0.001439
12	6	–0.000836	0.000099	0.000842
12	7	–0.000100	–0.000135	0.000168
12	8	–0.000231	0.000083	0.000245
12	9	–0.000283	0.000262	0.000386
12	10	0.000107	0.000396	0.000410
12	11	–0.000424	–0.000492	0.000650
12	12	0.000354	0.000118	0.000374
14	0	–0.000004	0.000000	0.000004
14	1	–0.000007	0.000008	0.000011
14	2	–0.000011	0.000015	0.000019
14	3	0.000003	–0.000002	0.000004
14	4	0.000001	0.000001	0.000001
14	5	0.000001	0.000001	0.000002
14	6	–0.000001	0.000000	0.000001
14	7	0.000003	–0.000001	0.000003
14	8	0.000000	0.000000	0.000001
14	9	0.000000	0.000001	0.000001
14	10	–0.000001	–0.000002	0.000002
14	11	0.000001	0.000002	0.000003
14	12	0.000000	0.000000	0.000000
14	13	0.000001	0.000000	0.000001
14	14	0.000001	0.000000	0.000001

[a] The CF parameters are only listed for positive values of q. The values with negative q are given by $B_{k-q} = (-1)^q B_{kq}^*$.

Table S8. Squared magnitudes of the projections of the *ab initio* CF eigenstates onto angular momentum eigenstates characterized by a total angular momentum $J = 15/2$ and an angular momentum projection M.

M	KD1		KD2		KD3		KD4		KD5		KD6		KD7		KD8	
–15/2	**0.847**	**0.144**	0.000	0.000	0.001	0.004	0.003	0.000	0.000	0.000	0.000	0.000	0.000	0.000	0.000	0.000
–13/2	0.000	0.000	**0.004**	**0.922**	0.011	0.049	0.002	0.000	0.004	0.004	0.001	0.001	0.000	0.002	0.000	0.000
–11/2	0.007	0.001	0.000	0.050	**0.141**	**0.600**	0.145	0.006	0.018	0.010	0.005	0.011	0.002	0.000	0.002	0.002
–9/2	0.000	0.000	0.000	0.007	0.025	0.124	**0.678**	**0.059**	0.031	0.030	0.013	0.006	0.005	0.017	0.003	0.001
–7/2	0.000	0.000	0.000	0.011	0.000	0.004	0.064	0.009	**0.445**	**0.402**	0.016	0.004	0.003	0.011	0.015	0.017
–5/2	0.000	0.000	0.000	0.001	0.005	0.022	0.002	0.000	0.021	0.010	**0.307**	**0.491**	0.092	0.020	0.017	0.011
–3/2	0.000	0.000	0.000	0.004	0.001	0.001	0.023	0.002	0.003	0.003	0.075	0.055	**0.114**	**0.702**	0.014	0.005
–1/2	0.000	0.000	0.000	0.002	0.008	0.005	0.001	0.005	0.008	0.011	0.004	0.010	0.000	0.032	**0.336**	**0.578**
1/2	0.000	0.000	0.002	0.000	0.005	0.008	0.005	0.001	0.011	0.008	0.010	0.004	0.032	0.000	**0.578**	**0.336**
3/2	0.000	0.000	0.004	0.000	0.001	0.001	0.002	0.023	0.003	0.003	0.055	0.075	**0.702**	**0.114**	0.005	0.014
5/2	0.000	0.000	0.001	0.000	0.022	0.005	0.000	0.002	0.010	0.021	**0.491**	**0.307**	0.020	0.092	0.011	0.017
7/2	0.000	0.000	0.011	0.000	0.004	0.000	0.009	0.064	**0.402**	**0.445**	0.004	0.016	0.011	0.003	0.017	0.015
9/2	0.000	0.000	0.007	0.000	0.124	0.025	**0.059**	**0.678**	0.030	0.031	0.006	0.013	0.017	0.005	0.001	0.003
11/2	0.001	0.007	0.050	0.000	**0.600**	**0.141**	0.006	0.145	0.010	0.018	0.011	0.005	0.000	0.002	0.002	0.002
13/2	0.000	0.000	**0.922**	**0.004**	0.049	0.011	0.000	0.002	0.004	0.004	0.001	0.001	0.002	0.000	0.000	0.000
15/2	**0.144**	**0.847**	0.000	0.000	0.004	0.001	0.000	0.003	0.000	0.000	0.000	0.000	0.000	0.000	0.000	0.000

References:

1. S. M. Cendrowski-Guillaume, G. Le Gland, M. Nierlich, M. Ephritikhine, *Organometallics*, **2000**, *19*, 5654-5660.
2. (a) A. Sekiguchi, T. Matsuo, H. Watanabe, *J. Am. Chem. Soc.* **2000**, *122*, 5652-5653. (b) T. Matsuo, A. Sekiguchi, *Bull. Chem. Soc. Jpn*., **2004**, *77*, 211-226.
3. B. M. Day, F. Guo, S. R. Giblin, A. Sekiguchi, A. Mansikkamäki, R. A. Layfield, *Chem. Eur. J.*, **2018**, *24*, 16779-16782.
4. A. Chakraborty, B. M. Day, J. P. Durrant, M. He, J. Tang and R. A. Layfield, *Organometallics*, 2020, ***39***, 8-12.
5. O. V. Dolomanov, L. J. Bourhis, R. J. Gildea, J. A. K. Howard, H. Puschmann, *J. Appl. Cryst.*, **2009**, *42*, 339-341.
6. G. M. Sheldrick, *Acta Cryst.*, **2015**, *A71*, 3-8.
7. G. M. Sheldrick, *Acta Cryst.*, **2015**, *C71*, 3-8.
8. D. Gatteschi, R. Sessoli, J. Villain, *Molecular Nanomagnets* (Oxford Univ. Press, 2006).
9. Gaussian 09, Revision E.01, M. J. Frisch, G. W. Trucks, H. B. Schlegel, G. E. Scuseria, M. A. Robb, J. R. Cheeseman, G. Scalmani, V. Barone, G. A. Petersson, H. Nakatsuji, X. Li, M. Caricato, A. Marenich, J. Bloino, B. G. Janesko, R. Gomperts, B. Mennucci, H. P. Hratchian, J. V. Ortiz, A. F. Izmaylov, J. L. Sonnenberg, D. Williams-Young, F. Ding, F. Lipparini, F. Egidi, J. Goings, B. Peng, A. Petrone, T. Henderson, D. Ranasinghe, V. G. Zakrzewski, J. Gao, N. Rega, G. Zheng, W. Liang, M. Hada, M. Ehara, K. Toyota, R. Fukuda, J. Hasegawa, M. Ishida, T. Nakajima, Y. Honda, O. Kitao, H. Nakai, T. Vreven, K. Throssell, J. A. Montgomery, Jr., J. E. Peralta, F. Ogliaro, M. Bearpark, J. J. Heyd, E. Brothers, K. N. Kudin, V. N. Staroverov, T. Keith, R. Kobayashi, J. Normand, K. Raghavachari, A. Rendell, J. C. Burant, S. S. Iyengar, J. Tomasi, M. Cossi, J. M. Millam, M. Klene, C. Adamo, R. Cammi, J. W. Ochterski, R. L. Martin, K. Morokuma, O. Farkas, J. B. Foresman, and D. J. Fox. *Gaussian, Inc.*, Wallingford CT, **2016**.
10. a) J. P. Perdew, K. Burke, M. Ernzerhof. *Phys. Rev. Lett.*, **1996**, *77*, 3865–3868; b)J. P. Perdew, K. Burke, M. Ernzerhof. *Phys. Rev. Lett.*, **1996**, *78*, 1396; c) M. Ernzerhof, G. E. Scuseria. *J. Chem. Phys.* **1999**, 119, 5029–5036; d) C. Adamo, V. Barone. *J. Chem. Phys.* **1999**, 110, 6158–6170
11. a) M. Dolg, H. Stoll, A. Savin, H. Preuß. *Theor. Chim. Acta.* **1989**, *75*, 173–194; b) D. Andrae, U. Häußermann, M. Dolg, H. Stoll, H. Preuß. *Theor. Chim. Acta.* **1990**, *77*, 123–141.
12. A. Schäfer, C. Huber, R. Ahlrichs. *J. Chem. Phys.*, **1994**, *100*, 5829–5835.
13. I. F. Galván, M. Vacher, A. Alavi, C. Angeli, F. Aquilante, J. Autschbach, J. J. Bao, S. I. Bokarev, N. A. Bogdanov, R. K. Carlson, L. F. Chibotaru, J. Creutzberg, N. Dattani, M. G. Delcey, S. S. Dong, A. Dreuw, L. Freitag, L. M. Frutos, L. Gagliardi, F. Gendron, A. Giussani, L. González, G. Grell, M. Guo, C. E. Hoyer, M. Johansson, S. Keller, S. Knecht, G. Kovačević, E. Källman, G. L. Manni, M. Lundberg, Y. Ma, S. Mai, J. P. Malhado, P. Å. Malmqvist, P. Marquetand, S. A. Mewes, J. Norell, M. Olivucci, M. Oppel, Q. M. Phung, K. Pierloot, F. Plasser, M. Reiher, A. M. Sand, I. Schapiro, P. Sharma, C. J. Stein, L. K. Sørensen, D. G. Truhlar, M. Ugandi, L. Ungur, A. Valentini, S. Vancoillie, V. Veryazov, O. Weser, T. A. Wesołowski, P.-O. Widmark, S. Wouters, A. Zech, J. P. Zobel, R. Lindh. *J. Chem. Theory Comput.*, **2019**, *15*, 5925–5964.
14. a) P.-O. Widmark, P.-Å. Malmqvist, B. O. Roos. *Theor. Chim. Acta*, **1990**, *77*, 1432–2234; b) B. O. Roos, R. Lindh, P.-Å. Malmqvist, V. Veryazov, P.-O. Widmark. *J. Phys. Chem. A*, **2004**, *108*, 2851–2858; c) B. O. Roos, R. Lindh, P.-Å. Malmqvist, V. Veryazov, P.-O. Widmark. *J. Phys. Chem. A*, **2005**, *109*, 6575–6579;d) B. O. Roos, R. Lindh, P.-Å. Malmqvist, V. Veryazov, P.-O. Widmark, A. C. Borin. *J. Phys. Chem. A.* **2008**, *112*, 11431–11435; e) B. O. Roos, V. Veryazov, P.-O. Widmark. *Theor. Chem. Acc.* **2004**, *111*, 345–351.
15. a) W. Kutzelnigg, W. Liu. *J. Chem. Phys.*, **2005**, *123*, 241102; b) M. Filatov. *J. Chem. Phys.* **2006**, *125*, 107101; c) . Daoling, M. Reiher. *Theor. Chem. Acc.,* **2012**, *131*, 1.
16. P. Å. Malmqvist, B. O. Roos, B. Schimmelpfenning. *Chem. Phys. Lett.*, **2002**, *357*, 230–240.
17. a) B. A. Heß, C. M. Marian, U. Wahlgren, O. Gropen. *Chem. Phys. Lett.*, **1996**, *251*, 365–371; b) O. Christiansen, J. Gauss, B. Schimmelpfennig. *Phys. Chem. Chem. Phys.*, **2000**, *2*, 965–971.
18. a) L. F. Chibotaru, L. Ungur. *J. Chem. Phys.*, **2012**, *137*, 064112; b) L. Ungur, L. F. Chibotaru. Computational *Modelling of Magnetic Properties of Lanthanide Compounds* in *Lanthanide and Actinides in Molecular Magnetism.* Eds. R. A. Layfield, M. Murugesu. Wiley,-VHC, Weinheim, Germany, **2015**.
19. L. Ungur, M. Thewissen, J.-P. Costes, W. Wernsdorfer, L. F. Chibotaru. *Inorg. Chem.*, **2013**, *52*, 6328–6337.
20. L. Ungur, L. F. Chibotaru. *Chem. Eur. J.* **2017**, *23*, 3708–3718.